

# Miscellaneous photometric variations in cataclysmic variables: V455 And, SS Cyg, AQ Men, LQ Peg, RW Tri and UX UMa<sup>1</sup>

Albert Bruch

Laboratório Nacional de Astrofísica, Rua Estados Unidos, 154,  
CEP 37504-364, Itajubá - MG, Brazil

(Published in: *New Astronomy*, Vol. 78, 101369 (2020))

## Abstract

Cataclysmic variables are among the photometrically most unstable stars in the zoo of stellar objects, exhibiting light variations on all time-scales between millennia and seconds. The literature is full of reports on variable phenomena which often require independent confirmation before they can be accepted as established facts. In this contribution I investigate accounts on miscellaneous variable features observed in six cataclysmic variables, drawing for this purpose largely on archival data, most of which have not been investigated in detail in the past, and complementing these data with some new observations. This enabled to confirm and expand upon some hitherto unconfirmed features in the light curves of these star, as well as the rejection of some others, while in still other cases an unambiguous answer to questions arising from previous papers was not possible.

Keywords: Stars: Binaries: Close – Stars: Novae, Cataclysmic variables – Stars: Dwarf novae – Stars: Individual: V455 And; SS Cyg; AQ Men; LQ Peg; RW Tri; UX UMa

## 1 Introduction

Among the many types of variable stars the cataclysmic variables (CVs) arguably are the champions of variability. CVs are interacting binary systems consisting of a Roche-lobe filling late type star (the secondary) orbiting a white dwarf (the primary) and transferring matter to the latter which forms an accretion disk before it settles onto the compact object (unless the magnetic field of the primary is strong enough to guide it directly to its surface). For a thorough review of the properties of CVs, see, e.g., Warner (1995). Variable phenomena occur in these systems periodically, quasi-periodically or irregularly on all times-scales from millennia to decades (outbursts of classical and recurrent novae), years, month and weeks (high and low states, dwarf nova outbursts), days and hours (orbital variations, superhumps

---

<sup>1</sup>Based partially on observations taken at the Observatório do Pico dos Dias / LNA

and beat phenomena between them), minutes and seconds (white dwarf rotation, flickering, quasi-periodic oscillations, dwarf nova oscillations).

Their thorough observation and characterization permits to elucidate many aspects of the nature of CVs in general as well as in individual systems. The literature is, however, full of reports on details which remain unconfirmed and may or may not represent true features in the investigated stars. If they are not, taking them at face values easily leads to confusion and miss-interpretations. It is therefore worthwhile to use additional data in order to verify unconfirmed claims of variable features observed at one instance or the other. Fortunately, a lot of such and so far little or not studied data are available in public data archives.

Using such data and complementing them with some new dedicated observations, I investigate in this small contribution miscellaneous variations in six CVs (some better and some less well known) in order to verify previous unconfirmed features and to add some new details concerning their temporal behaviour on time-scales of seconds to weeks. V455 And is an intermediate polar. Here, the orbital period, the occurrence of superhumps, and the temporal behaviour of high frequency oscillations are investigated (Sect. 3). SS Cyg (Sect. 4) is the prototype of the dwarf nova class of CVs. Some details about its orbital modulations are studied along with variations at higher frequencies. Orbital variations and a possible modulation with a period of some days in the novalike variable AQ Men are looked at in Sect. 5, while controversies in the literature about variations on hourly time-scales in the VY Scl star LQ Peg are discussed in Sect. 6. A follow-up on recent reports of superhumps and of oscillations on time-scales of weeks in RW Tri is presented in Sect. 7. Finally, in Sect. 8 it is verified if superhumps observed in UX UMa in 2015 are also present at other epochs.

## 2 The data

The data used in this study consist of light curves which in most cases span several hours and have a time resolution of (with a few exceptions) better than one minute (down to 5 s). Most of them were retrieved either from the AAVSO (American Association of Variable Star Observers) International Database or from the Centre de Données Astronomique de Strassbourg (CDS). Only for AQ Men new and so far unpublished observations are used. Details about the data are given in the sections concerning the individual objects. Whenever light curves of different nights were combined, the time stamps of all data points were first transformed into barycentric Julian Date on the Barycentric Dynamical Time scale, using the online tool of Eastman et al. (2010) in order to remove any light travel time differences in the solar system. This was not necessary if the archival data already included the heliocentric correction (thus neglecting the small difference between barycentric and heliocentric time). Since the AAVSO data were observed by a variety of observers with different instruments, the details of which are not known, the magnitude scale can differ between the data sets and night-to-night variations seen in the light curves may not be real. Therefore, unless stated otherwise the average magnitude has been subtracted from these light curves before further processing.

## 3 V455 Andromedae

V455 And is a comparatively well studied system. Even so, additional data still can add to our knowledge of the star, confirming and substantiating previous observations. Discovered in the Hamburg Quasar Survey (Hagen et al., 1995) as HS2331+3905, it is considered a

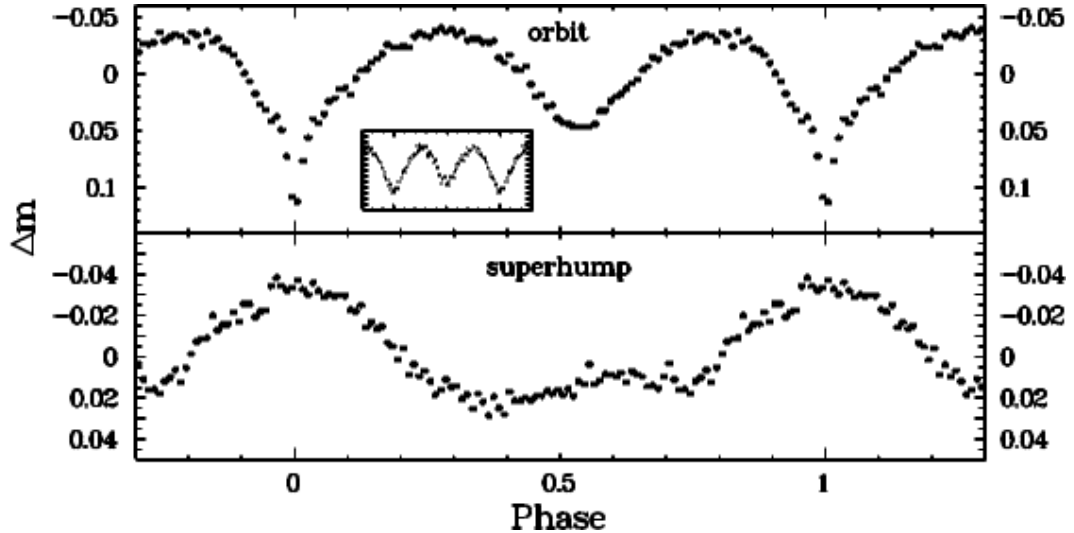


Figure 1: Average waveform of the orbital (top) and superhump (bottom) variations of V455 And. The insert in the upper frame results from folding the light curves on the  $1 \text{ d}^{-1}$  alias of half the orbital period (see text for details).

DQ Her type intermediate polar with a short orbital period of 81.08 min (Araujo-Betancor et al., 2005). It is also a dwarf nova of the WZ Sge subtype with only one outburst having been observed so far (Nogami et al., 2009; Maehara et al., 2009; Matsui et al., 2009). The orbital light curve is very similar to that of WZ Sge. It is double humped and contains a shallow grazing eclipse. Moreover, Araujo-Betancor et al. (2005) detected a positive superhump during quiescence, while Kozhevnikov (2015) observed a negative superhump. A puzzling feature is a 3.5 h spectroscopic period detected by Araujo-Betancor et al. (2005) which is in no way related to the orbital period.

In the high frequency regime several periods were first observed in V455 And by Araujo-Betancor et al. (2005) and later studied in more detail by other authors. A signal on time-scales of 5–6 min which changes slightly from night to night is interpreted as non-radial pulsations of the white dwarf. A coherent 1.12 min signal is thought to be the rotation period of the primary star. A precise period of  $P_{\text{spin}} = 67.61970396 \text{ s}$  has been measured by Mukadam et al. (2016). Closely related is another, slightly drifting period of 67.20 s, first mentioned by Gänsicke (2007) who interpreted it as being due to the illumination by the rotating white dwarf of a warped inner accretion disk precessing retrogradely. Intriguingly, the beat period between the latter and  $P_{\text{spin}}$  is very close to the 3.5 h radial velocity variation.

The observational data used for this study were retrieved from AAVSO International Database. They consist of 116 light curves with a duration between 77 and 958 min and a time resolution between 20 and 169 s, all referring to quiescence. They were obtained in the eleven observing seasons between 2008 and 2018.

### 3.1 The orbital period

The orbital period of V455 And is known to a rather high accuracy (Araujo-Betancor et al., 2005). However, the longer time base of the present data permits an even better determination. For that purpose the light curves of each observing season between 2008 and 2018 (except 2017 when only one light curve was observed) were combined and then folded on

the orbital period. This enabled an unambiguous detection of the grazing eclipses which are not obvious in individual light curves. For each season an eclipse epoch was determined by fitting a sixth order polynomial to the eclipse in the folded light curve. The period of Araujo-Betancor et al. (2005) is more than good enough to maintain cycle counts over the entire time base, permitting thus to associate a cycle number to each of the 10 eclipse epochs. A linear least squares fit, including also the eclipse epoch informed in eq. 1 of Araujo-Betancor et al. (2005) and weighting each epoch with the total observing time of each season, then yields the improved ephemeris:

$$T_{\text{ecl}} = \text{BJD}2454623.52003(9) + 0.056309188(2) \times E$$

where the errors are the formal fit errors. The light curve folded on the period and binned in phase intervals of width 0.01 is shown in the upper frame of Fig. 1. Not astonishingly, the waveform is very similar to that shown in Fig. 7 of Araujo-Betancor et al. (2005): the first maximum extends from phase 0 to 0.534 and is thus slightly longer than the second maximum. At 0.084 mag (measured from its peak to the bottom of the secondary minimum) it has a slightly lower amplitude than the second maximum which reaches 0.081 mag. However, it should be noted that the relative amplitudes of the maxima may change from season to season, as is obvious from fig. 5 of Kozhevnikov (2015). The eclipse depth, defined here as the magnitude difference between the secondary minimum and the eclipse bottom, is 0.062 mag.

### 3.2 The superhumps

Claims have been put forward concerning the presence of positive as well as negative superhumps in V455 And. In observations obtained between 2000 and 2003, Araujo-Betancor et al. (2005) observed a periodic modulation with a period of 83.38 min (or an alias at 88.51 min), slightly longer than the orbital period, which they interpret as a positive superhump. It is not seen in observations taken in 2013 and 2014 by Kozhevnikov (2015) who, instead, found a modulation with a period of 80.376 min, slightly shorter than the orbital period. He considers this variation as a negative superhump.

The reality of the positive superhump may be questioned. First, it has a double humped structure (see Fig. 8 of Araujo-Betancor et al., 2005), quite unusual for ordinary superhumps in CVs. While there may be some additional structure in the waveform, the numerous examples shown by Kato et al. (2009) and in other papers of that series clearly show one dominant maximum during each superhump cycle. More important, however, is the remarkable proximity of half of the alleged superhump period (41.69 min) to the  $1 \text{ d}^{-1}$  alias of the main power spectrum signal (41.72 min, i.e., half the orbital period). Folding the present light curves on the  $1 \text{ d}^{-1}$  alias of the orbital period, as shown in the insert in the upper frame of Fig. 1, smears out the eclipses, leading to a waveform with two minima of slightly different depth. This is quite similar to fig. 8 of Araujo-Betancor et al. (2005). Therefore, the corresponding variations can easily be explained by an aliasing effect and there is no need to invoke the presence of a permanent superhump during quiescence of this WZ Sge star.

In the present data, a possible positive superhump can at most marginally be seen during some years, while the negative superhump is detected during most observing seasons. This is shown in Fig. 2 which contains the Lomb-Scargle periodograms (Lomb, 1976; Scargle, 1982; hereafter also referred to as power spectra) of the combined seasonal light curves, noting that those of 2011 and 2014 are based on only three nights of observations, which explains their peculiar appearance. The broken vertical lines indicate (from left to right)

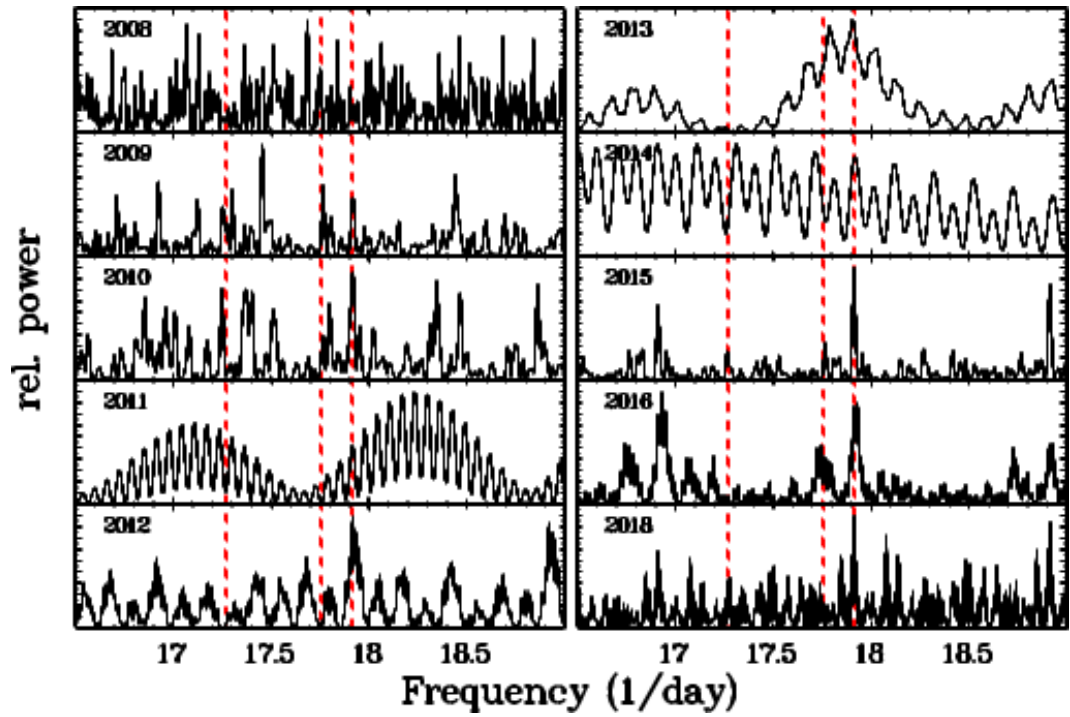


Figure 2: Periodograms of the combined light curves of V455 And during various observing seasons. The broken vertical lines indicate (from left to right) the frequencies of the alleged positive superhump at 83.38 min (Araujo-Betancor et al., 2005), the orbit, and the negative superhump detected by Kozhevnikov (2015).

the frequencies of the alleged positive superhump (Araujo-Betancor et al., 2005), the orbit, and the negative superhump (Kozhevnikov, 2015).

While the orbital frequency appears only weakly during some seasons (remembering that due to the double humped light curve the bulk of the power is concentrated at twice the orbital frequency), a significant signal is present at the negative superhump frequency (and its  $1 \text{ d}^{-1}$  aliases) in all seasons except 2008 and 2011. The average of the peak frequencies in the yearly periodograms yields a superhump period of  $80.382 \pm 0.018 \text{ min}$ , entirely consistent with the value measured by Kozhevnikov (2015).

In order to obtain the waveform of these variations, a least squares sine fit with the period fixed to half the orbital period was subtracted from the combined seasonal light curves in order to remove (at least partly) the orbital variations. The result was then folded on the superhump period measured during that particular season, adjusting the phase such that the maximum of the waveform has phase 0. The average waveform, binned in phase intervals of width 0.01, is shown in the lower frame of Fig. 1. Just as observed by Kozhevnikov (2015) (see his fig. 5) the superhump has two maxima. However, the intermediate hump at phase 0.6 has a much smaller amplitude in the present data. The total amplitude of the main hump is  $\approx 0.057 \text{ mag}$  which is significantly less than estimated from fig. 5 of Kozhevnikov (2015).

Finally, testing if the superhump can be described by a single period, constant over several years, an attempt was made to find a value for the period which keeps the superhump maximum in phase over the entire time base of the data. This turned out not to be possible, indicating that either the period or the phase (or both) undergo real variations, however small, over time.

### 3.3 The pulsations

First noticed by Araujo-Betancor et al. (2005), multiple signals in the power spectra of V455 And, corresponding to periods in the 4–6 min range, have been studied subsequently also by Gänsicke (2007), Silvestri et al. (2012) and Szkody et al. (2013). While most authors consider them as due to non-radial pulsations of the white dwarf, Szkody et al. (2013) question this view based on indications for an origin away from the white dwarf photosphere.

None of the cited studies was able to isolate specific frequencies. The number of significant signals and their frequencies changes from night to night, only permitting to identify a range for their occurrence, and this range is not even constant over time. Szkody et al. (2013) observed an evolution of the pulsation period from  $\approx 4.2 \text{ min}$  in 2009 (two years after the dwarf nova outburst of V455 And) to  $\approx 5.5 \text{ min}$  in 2012. The latter value is similar to that measured by Araujo-Betancor et al. (2005) in 2000 – 2003 and Gänsicke (2007) in 2004, i.e., years before the outburst. Szkody et al. (2013) attribute the change of preferred periods to the cooling of the white dwarf surface after being heated during the eruption.

The present data permit to document the evolution of the range of pulsation periods over a longer time base. For this purpose, Fig. 3 shows the relevant frequency interval of the periodograms calculated from the combined seasonal light curves. All are drawn on the same scale. If there is a preferred range of frequencies at all in 2008, it is very broad. However the periodogram may also be compatible with the absence of well defined pulsations. The picture becomes clearer in the subsequent years, where a trend for pulsations from higher to lower frequencies is evident, confirming the findings of Szkody et al. (2013). This trend comes to a halt in 2012, when the range of frequencies has reached that observed in 2000–2004. Thereafter, it remains constant until 2018. In line with the explanation for the period evolution forwarded by Szkody et al. (2013), the white dwarf in V455 And may still have been

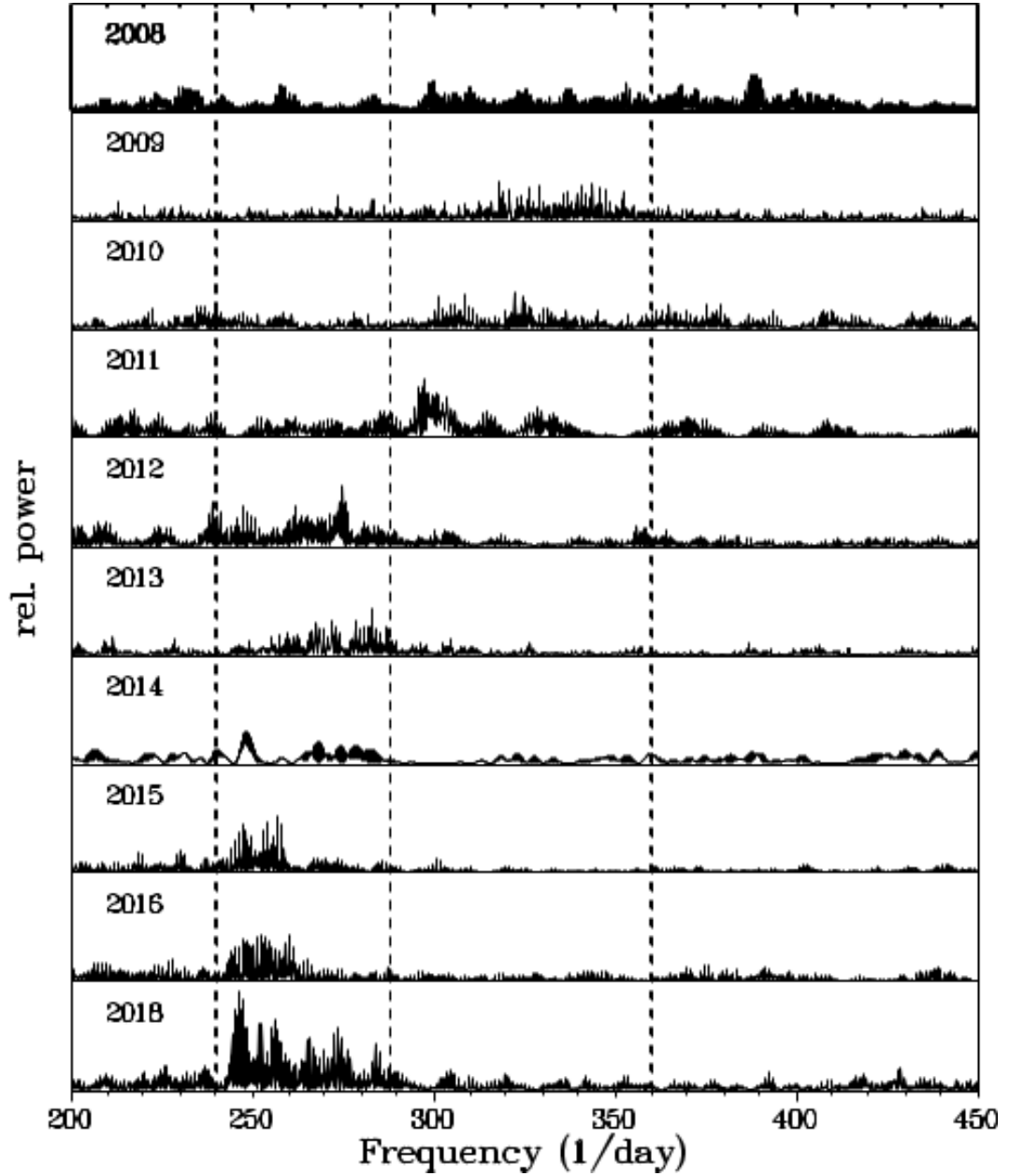


Figure 3: Periodograms of the combined light curves of V455 And during various observing seasons, covering the frequency range of the white dwarf pulsations. All periodograms are drawn on the same vertical scale. The broken vertical lines indicate (from right to left) frequencies corresponding to 4, 5 and 6 min.

to hot to permit non-radial pulsations in 2008 and has reached its equilibrium temperature by 2012.

Conventional Fourier techniques, using long light curves, cannot reveal the duration and evolution of specific pulsations over time. Stacked power spectra permit a more detailed view of their evolution over the time-scale of hours. For this purpose I selected some nightly light curves, the periodograms of which contain comparatively strong signals in the frequency range of the non-radial pulsations. Periodograms of sections of these data trains, 36 min long, were constructed, allowing for an overlap of 90% between subsequent sections. The individual power spectra were then stacked on top of each other, resulting in a 2D representation (frequency vs. time; for a more detailed description of this technique, see Bruch, 2014). The results are shown in Fig. 4. The double arrow at the left indicates the length of the data sections used to calculate the individual spectra. Thus, any vertical structures in the 2D images smaller than this are not independent from each other.

The figure shows that pulsations can persist over several hours, sometimes with a systematic shift in frequency and, in general, considerable variations of the amplitude. This can lead to multiple peaks in the conventional periodograms, complicating their interpretation severely. Moreover, isolated events in the light curve, lasting for only a short time, can generate strong signals in the periodogram which may easily be mistaken as evidence for persistent pulsations. Some examples are shown in Fig. 5. It is therefore not astounding that so far no systematics have been detected in the occurrence of these pulsations which would permit a better characterization.

### 3.4 The spin variations

In the high frequency regime, V455 And exhibits a stable oscillation with a period of 67.62 s and its harmonic at half this value, first seen by Araujo-Betancor et al. (2005). It is accompanied by a slightly incoherent signal at 67.24 s. Their frequency difference corresponds to the 3.5 hr spectroscopic period. The stable period is identified with the white dwarf rotation, while Gänsicke (2007) interprets the 67.24 s period as due to the illumination of structures in the inner disk. These variations have also been studied spectroscopically by Bloemen et al. (2013), and photometrically by Silvestri et al. (2012) and, more thoroughly, by Mukadam et al. (2016).

The present data cannot add much to this. Of the 116 light curve only 18 have a time resolution sufficient to resolve the white dwarf spin period (and none to resolve its harmonic). Most of them were observed in 2016-18. A significant signal is seen in the periodogram of all suitable light curves at an average period of  $67.304 \pm 0.020$ . This is in between the spin period and its satellite period. Tests with artificial signals at the two periods, sampled in the same way as the real light curves, show that the capacity to resolve them in the periodograms depends on their amplitude ratio as well as their relative phases. Mukadam et al. (2016) observed a ratio of 3-4 for the amplitudes of the 67.24 and 67.62 s signals. In the present data such a ratio inhibits the resolution of the two periods and shifts the corresponding periodogram peak to a value slightly longer than 67.24 s. Thus, the present results are entirely consistent with results obtained in earlier observing seasons.

## 4 SS Cygni

As the prototype dwarf nova and one of the brightest members of its class SS Cyg is arguably one of the best studied of all cataclysmic variables. Even so, a detailed look at available observations may shed some additional light on the structure and behaviour of the system.



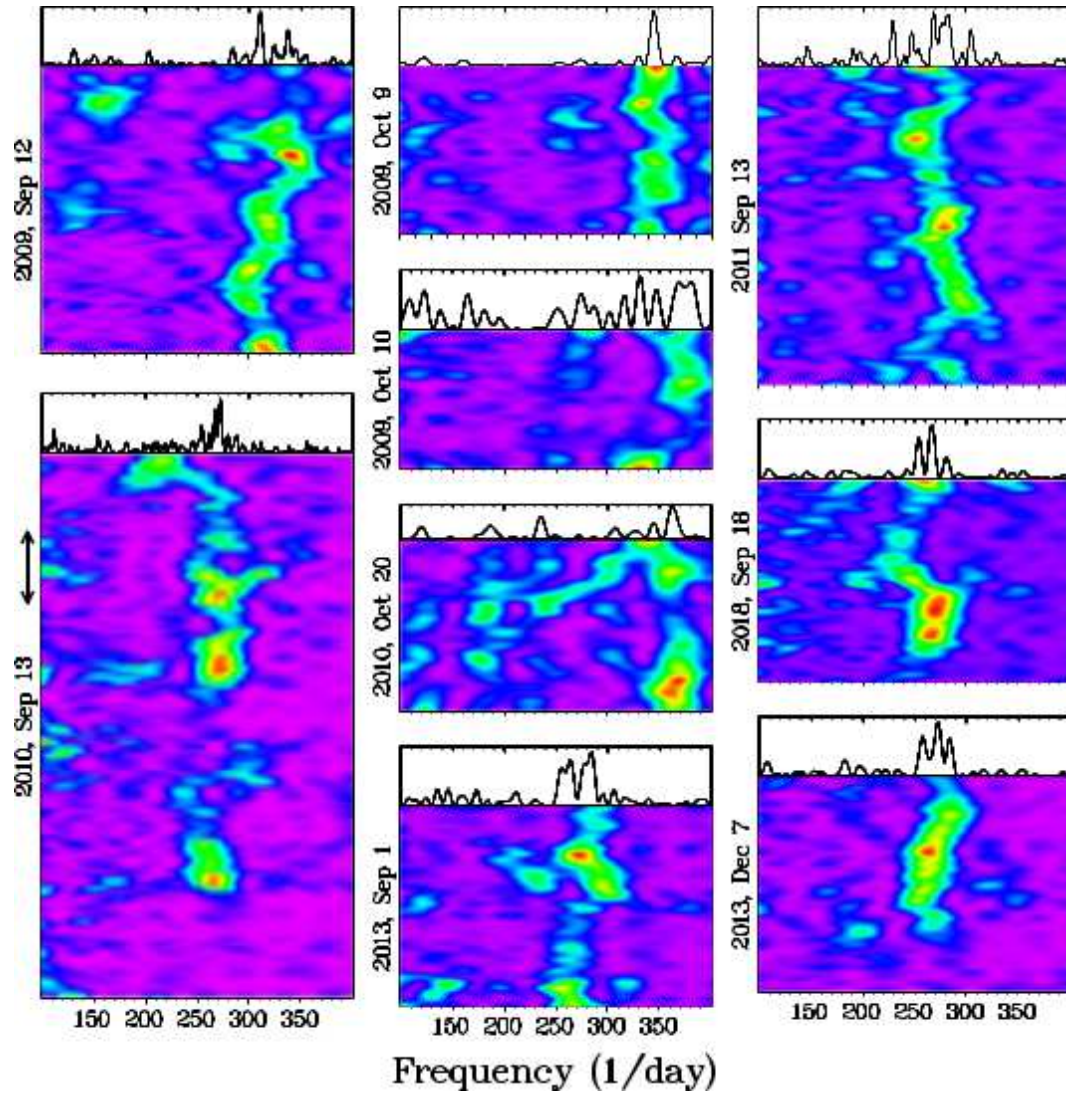


Figure 4: Stacked power spectra of some light curves of V455 And, illustrating the evolution of the non-radial pulsations over time. Time increases from bottom to top. The double arrow at the left, corresponding to 36 min, indicates the length of data sections used to calculate the power spectra. Above each spectrum the conventional Lomb-Scargle periodogram, using the entire light curve, is shown.

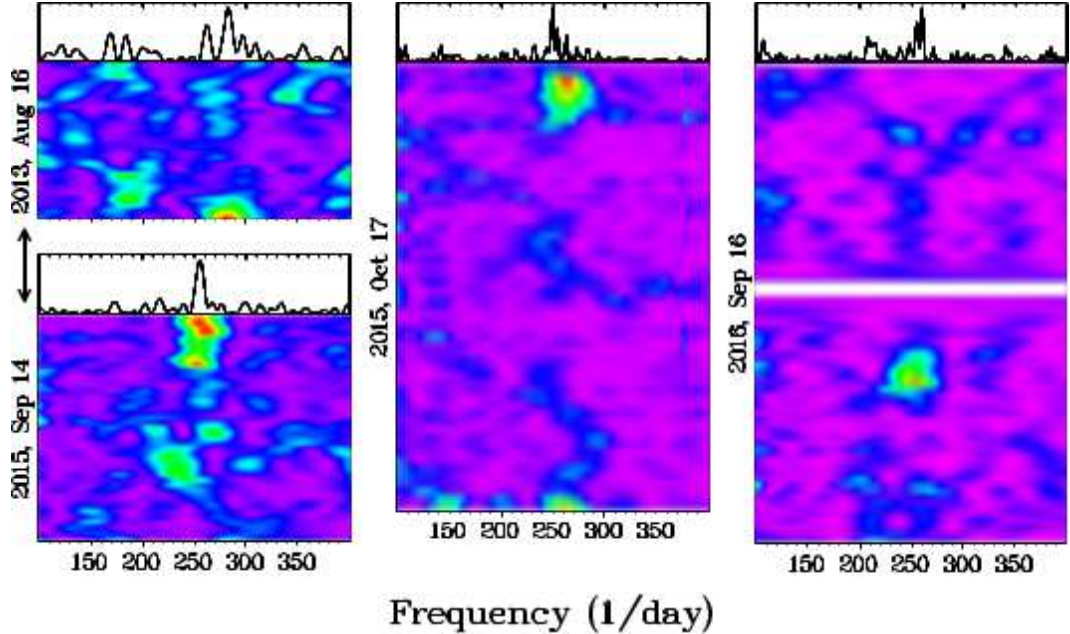


Figure 5: Stacked power spectra of some light curves of V455 And, illustrating cases in which pulsations occurring during short time intervals generate strong signals in conventional periodograms. The figure is organized in the same way as Fig. 4. (The gap in the spectrum at the right reflects a gap in the light curve.)

Here, I will investigate the shape of orbital variations in the light curve and its supposed variations, and the reality of alleged  $\approx 12$  min oscillations associated with the white dwarf rotation.

SS Cyg has a comparatively long orbital period. The most accurate available value of 0.27512973 d is based on spectroscopic measurements of Hessman et al. (1984). Although published three and a half decades ago, the formal error amounts to a phase uncertainty of only about 0.02 to the present day, which is negligible in the context of this study.

The data used here consist of 89 *V* band light curves, all observed during quiescence, retrieved from the AAVSO International Database. They refer to the time interval between 2005 and 2015, and have a duration between 1 and 10 h at a time resolution of 22 to 183 s.

#### 4.1 Orbital variations

Orbital variations in SS Cyg are often not as obvious as in other systems and may be hardly significant in an individual light curve in the presence of strong flickering. However, when folding various light curves on the orbital period, a waveform with two humps of different height appears. This has first been noted by Voloshina & Lyutyi (1983) and has also been documented by Bartolini et al. (1985), Voloshina (1986), Bruch (1990), Voloshina & Lyutyi (1993), Kjurkchieva et al. (1998) and Voloshina & Khruzina (2000). The large amount of the data investigated here permit a more rigorous characterization of these variations.

For this purpose, all light curves were folded on the orbital ephemeris of Hessman et al. (1984). Combining them into a single phase folded light curves provided a first approximation of the orbital waveform. This is slightly blurred because subtracting simply the nightly

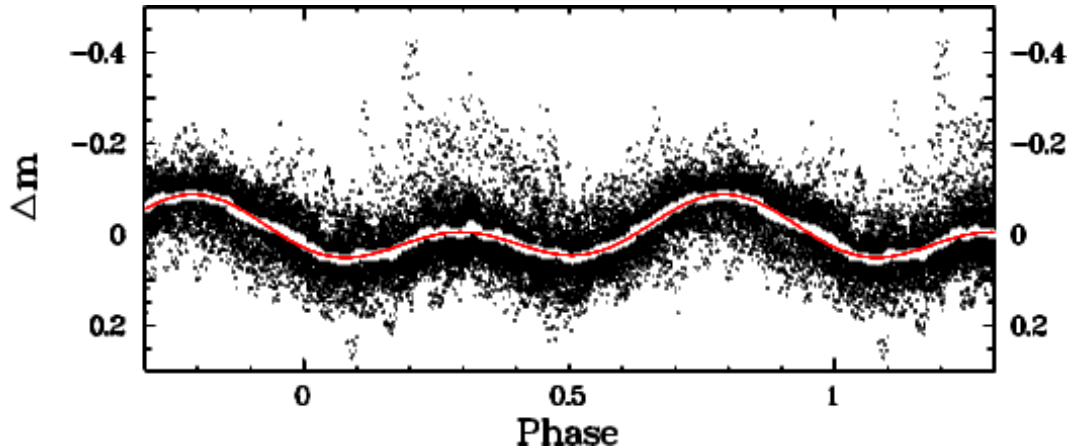


Figure 6: All light curves of SS Cyg folded on the orbital period. The white ribbon represents a binned version of the same data, using phase bins of width 0.01. The red curve is a two component least squares sine fit with periods fixed to 1 and 0.5. Phase 0 corresponds to the inferior conjunction of the red dwarf.

average magnitude from the original light curve (Sect. 2) does not only remove night-to-night variations, but also a part of the orbital variations if the length of a light curve is not an integer multiple of the orbital period. However, it is good enough to provide a correction which depends on the phase coverage of each light curve and which was then applied. The combined phase folded light curves after this correction provided a cleaner waveform which is shown in Fig. 6 (black dots). The white ribbon represents a binned version of the same data, using bins of width 0.01 in phase. Phases are defined such that the zero point corresponds to the inferior conjunction of the red dwarf.

The variations can well be described by the superposition of two sine waves with periods equal to the orbital period and half that value (red graph in the figure), leading to a waveform with two humps of unequal height separated by minima of almost equal depth. The slightly deeper minimum occur at phase 0.08, just after the conjunction of the stellar components. The separation of the minima is 0.425 in phase which means that the second (higher) hump is somewhat broader than the first. Its total amplitude is 0.1 mag. All these properties agree well with the mean light curve shown in fig. 2 of Voloshina & Khruzina (2000).

The main hump has its maximum at phase 0.79, close to where in many high inclination CVs a maximum is seen, interpreted as being caused by the changing visibility of the point of impact on the accretion disk of the stream of matter transferred from the secondary (i.e., the hot spot). Thus, it is close at hand to interpret the entire light curve as a superposition of variable visibility of the hot spot and some other structure which (Bitner et al., 2007) identify with ellipsoidal variations of the secondary star (with expected maxima of equal height at phases 0.25 and 0.75). However, this cannot be the whole story because in that case due to the decreasing contribution of the cool secondary star at shorter wavelengths the phase 0.25 maximum should be considerably fainter in the *B* compared to the *V* band, and even more so in the *U* band, contrary to the almost constant amplitude in all bands observed by Voloshina (1986), Voloshina & Lyutyi (1993) and Voloshina & Khruzina (2000). Moreover, double humped orbital light curves are also observed in short period CVs where the secondary does not contribute perceptibly to the visual light and ellipsoidal variations can therefore not explain the waveform. Examples are V455 And (see Fig. 1) and WZ Sge

Table 1: Amplitudes of a two component sine fit to the orbital variations of SS Cyg with periods fixed to the orbital period  $P_{\text{orb}}$  and to  $P_{\text{orb}}/2$  measured in different years.

Year	A ( $P_{\text{orb}}$ ) (mag)	A ( $P_{\text{orb}}/2$ ) (mag)	$N_{\text{LC}}^*$	$\Delta T^{**}$ (h)
2005	0.012	0.049	4	9.5
2006	0.056	0.056	34	138.7
2007	0.055	0.028	5	27.1
2009	0.005	0.060	16	78.0
2010	0.034	0.034	8	21.7
2011	0.035	0.031	6	14.4
2014	0.058	0.042	4	10.0
2015	0.071	0.038	11	61.4

$N_{\text{LC}}^*$  number of light curves  
 $\Delta T^{**}$  total time base of light curves

(e.g., Patterson et al., 2018).

Claims have been put forward by Voloshina (1986) and Voloshina & Lyutyi (1993) concerning a dependence of the shape of the orbital variations on the outburst phase of SS Cyg as well as the presence of narrow eclipses just before and after outbursts. These are based on a comparatively small number of light curves, meaning that a non-random distribution of strong flickering flares may mimic variability.

To address this question, I first investigate the average waveform as a function of observing season. This is done in Fig. 7 where the binned average orbital light curves in different years are shown together with the respective two component sine fit (red), and in Table 1 where the amplitude of the sine components are quoted together with the number of contributing light curves and the total time base of the data. The latter may provide a feeling of the statistical reliability of the results. Concentrating on those years with many data (and thus a well defined average waveform), i.e., 2006, 2009, and 2015, it is seen that the waveform indeed varies over time: In 2006 the main hump is about twice as high as the secondary hump; in 2009 both humps are of approximately equal height; and in 2015 the fainter hump is all but absent. Similar variations, albeit less clear, can also be seen in other years.

These results show that one must not mix data of various observing seasons in order to investigate dependencies of the waveform (and the presence of eclipses) on the phase in the outburst cycle. Therefore, I restrict myself for this purpose to the year with the largest number of available light curves, i.e., 2006. The AAVSO light curve of that observing season, binned in 1 d intervals, is reproduced in Fig. 8 (top), where the red vertical bars indicate the epochs of the time resolved light curves used here. Orbital phase folded light curves falling into the first, second and last third of each inter-outburst interval were averaged and are shown in the lower frame of the figure. No systematic differences are seen. There are indeed some low points in the average waveform of light curves observed just after outbursts at a phase consistent with the supposed eclipses seen by Voloshina & Lyutyi (1993). However, these can all be trace to one particular light curve (containing several gaps, arousing the suspicion of mediocre observing conditions), while several others covering the same phases do not contain this feature. Thus, the present data cannot confirm the presence of eclipses or variations of the orbital wave form as a function of phase in the outburst cycle.

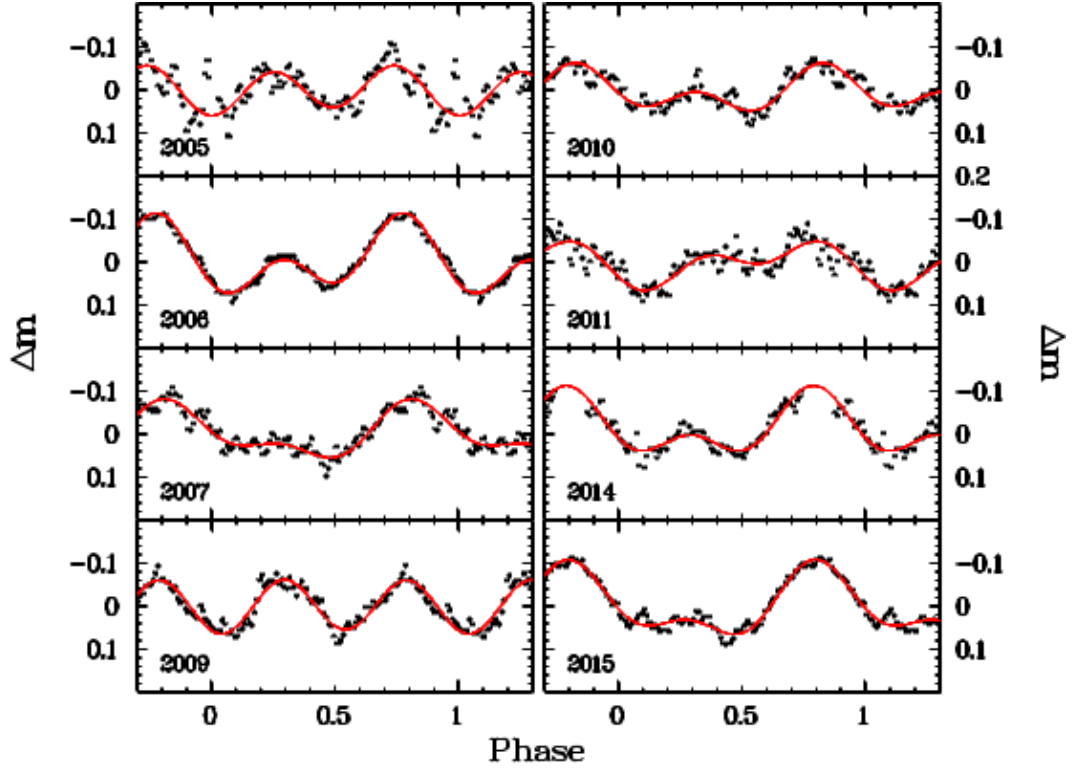


Figure 7: Light curves of SS Cyg folded on the orbital period and binned, separately for different observing seasons. The red curves are least squares fits with periods fixed to the orbital period and half that values.

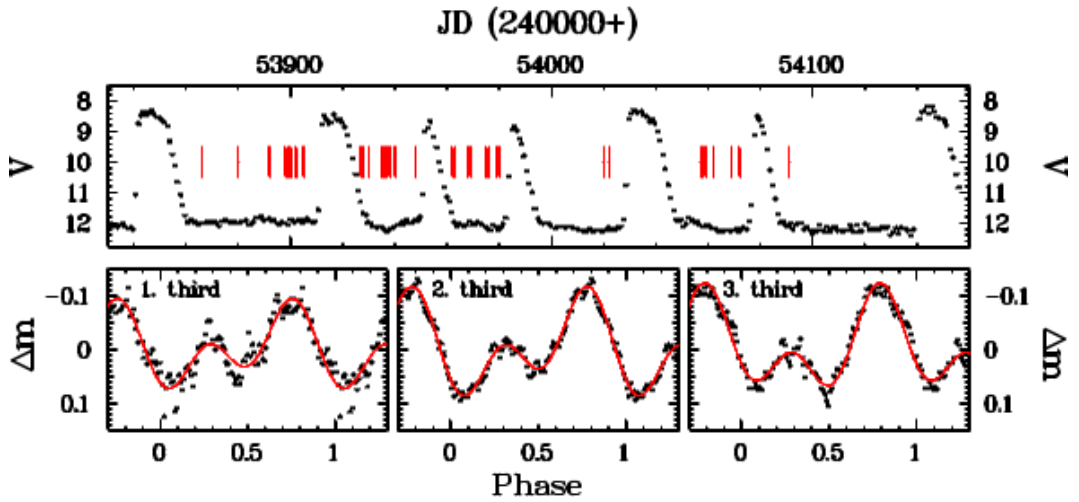


Figure 8: *Top*: AAVSO light curves of SS Cyg during the 2006 observing season, binned into 1 d intervals. The red vertical lines indicate the epochs of the nightly light curves used here. *Bottom*: Average waveform of the orbital variations in the first, second and last third of the inter-outburst intervals.

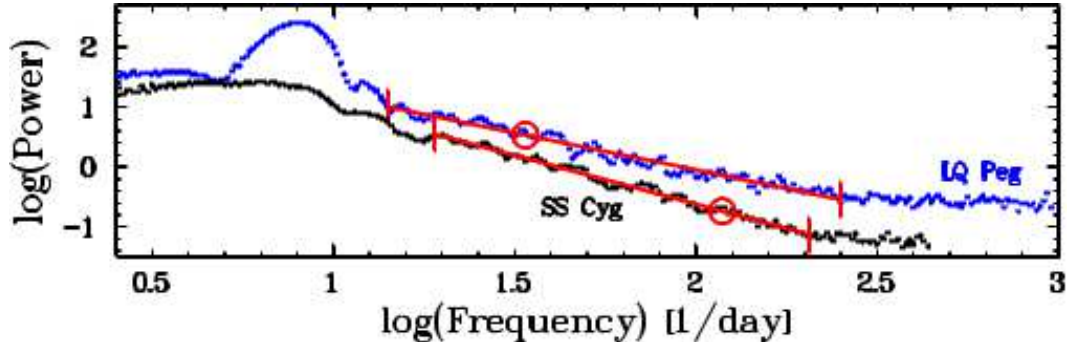


Figure 9: Average power spectra of SS Cyg and LQ Peg (the latter shifted upwards for clarity) on the double logarithmic scale. The red vertical bars indicate the limits of the red noise realm used to measure the spectral index  $\gamma$ , i.e., the slope of the red graph. The open circles mark the frequency of the supposed 12.18 min oscillations in SS Cyg and the centre of the range of QPOs suspected in LQ Peg.

## 4.2 SS Cyg at higher frequencies

Although not generally recognized as a magnetic system, claims have repeatedly been put forward in the past for SS Cyg to be an intermediate polar. An extensive list of arguments supporting this idea is enumerated by Giovannelli & Sabau-Graziati (2012) (see also references cited in that paper). One of these is the presence of variations with a period of 12.18 min which Giovannelli & Sabau-Graziati (2012) suspect to be the beat period between the white dwarf spin and the orbit. It has been observed by Bartolini et al. (1985) and is also mentioned in a theseis by V. Tramontana, cited by Giovannelli & Sabau-Graziati (2012), but unfortunately not readily available for verification. On the other hand, Bruch (1990) and Voloshina & Lyutyi (1993) could not confirm the reality of this signal.

Verifying this issue, using the more extensive data set studied here, the respective frequency range in power spectra of all light were investigated. In no case evidence for a periodicity close the 12 min was seen.

At high frequencies the power spectra of cataclysmic variable light curves are characterized by red noise caused by flickering, meaning that  $P \propto f^{-\gamma}$ , where  $P$  is the power,  $f$  the frequency and  $\gamma$  the spectral index. At very high frequencies white noise due to (approximately) Gaussian measurement errors takes over. On the double logarithmic scale, red noise causes a linear drop of the power with increasing frequency with a slope of  $-\gamma$ , and white noise results in a constant power level. Distinctive peaks or humps superposed upon this simple shape then indicate the presence of coherent or quasi periodic oscillations (QPOs) in a light curve.

Fig. 9 shows the average power spectrum of all light curves, binned into intervals of with 0.01 in  $\log(f)$ . The frequency of the supposed 12.18 min oscillations is marked by a red open circle. The figure confirms the absence of any clear signal at this frequency. Instead, the shape of the powerspectrum confirms the expectations: A linear decline is seen over a wide range. Within the bounds indicated by the red vertical marks (thus, avoiding the transition to the white noise realm at very high frequencies) the spectral index is measured to be  $\gamma = 1.62 \pm 0.18$ , where the error is the standard deviation of  $\gamma$  derived separately for the various observing seasons covered by the data.

## 5 AQ Mensae

The most basic parameter of any binary system is its orbital period. In most cases it is more or less straight forward to be measured. The most reliable methods are the determination of the radial velocity curve and – if the orbital inclination is suitable – the measurement of epochs of well defined eclipses. Often the light curves also exhibit more gradual brightness variations which reveal the orbital period. However, in binary systems with a complicated structure such as CVs permanent or transient features are sometimes observed which mimic orbital variations and can thus lead to false claims of orbital periods. One such case may be AQ Men.

AQ Men is a fairly bright ( $V \approx 14.3 - 15.3$ ) CV which so far has attracted little attention. The star was detected in the Edinburgh-Cape Blue Object Survey as EC 05114-7955 by Chen et al. (2001). They suspected a dwarf nova nature but did not exclude the possibility of AQ Men being a novalike variable. Armstrong et al. (2013) prefer a classification as a novalike variable, based on the absence of observed outbursts even many years after discovery, and on the compatible spectrum.

From radial velocity variations Chen et al. (2001) derived a period of  $P_{\text{sp}} = 0.130 \pm 0.014$  d. Considering that the total time base of their observations covers only 1.5 periods the quoted error may be underestimated. Moreover, the authors did not show a radial velocity curve, making it difficult to assess the reliability of the derived period. Within the error, the spectroscopic period is consistent with periods found in extensive photometric observations by Armstrong et al. (2013). They suspected the presence of grazing eclipses in the light curve of AQ Men, recurring with a period of  $P_{\text{ecl}} = 0.141471$  d. These eclipses are so shallow that in most cycles they cannot readily be distinguished in the presence of considerable flickering activity and only appear more clearly in a phase folded light curve. Armstrong et al. (2013) also found a photometric variation with a period of  $P_{\text{nSH}} = 0.13646$  d and a full amplitude of  $\sim 0.07$  mag (see fig. 3 of Armstrong et al., (2013)). The period being slightly shorter than the eclipse (and thus orbital) period, the authors consider this modulation as being due to a negative superhump. Finally, Armstrong et al. (2013) claim the presence of a longer period of 3.78 d with a full amplitude of  $\sim 0.12$  mag (their fig. 3).

I used the 60 cm Boller & Chivens telescope of the Observatório do Pico dos Dias, Brazil, to observe AQ Men in 8 nights between 2018, September 6 and 16. Light curves in unfiltered light spanning between 100 and 126 min (except for one shorter run of 30 min) were obtained at a time resolution of 5 sec. Synthetic aperture photometry was performed on the original images taken with a blue sensitive CCD IKon-L936-BEX2-DD. Magnitudes were measured relative to the primary comparison star UCAC4 051-003195 (Zacharias et al., 2013) ( $V = 14.931$ ). For cataclysmic variables the throughput of the instrumentation corresponds roughly to  $V$  (Bruch, 2018). The light curves are shown in Fig. 10 where the time and magnitude scales are the same for all frames. They are characterized by flickering, variations on the time-scale of the length of each observing run, and night-to-night variations.

### 5.1 Night-to-night variations

The night-to-night variations are not random but appear to be systematic. This is shown in Fig. 11, where the combined light curves of all observing nights are plotted. The dots beneath the light curve represent the nightly averages of the difference between the primary comparison star to AQ Men and a check star (shifted in magnitude by an arbitrary constant). It is virtually constant, attesting to the significance of the night-to-night variations of AQ Men. A formal least squares sine fit (red curve in the figure) yields a full amplitude

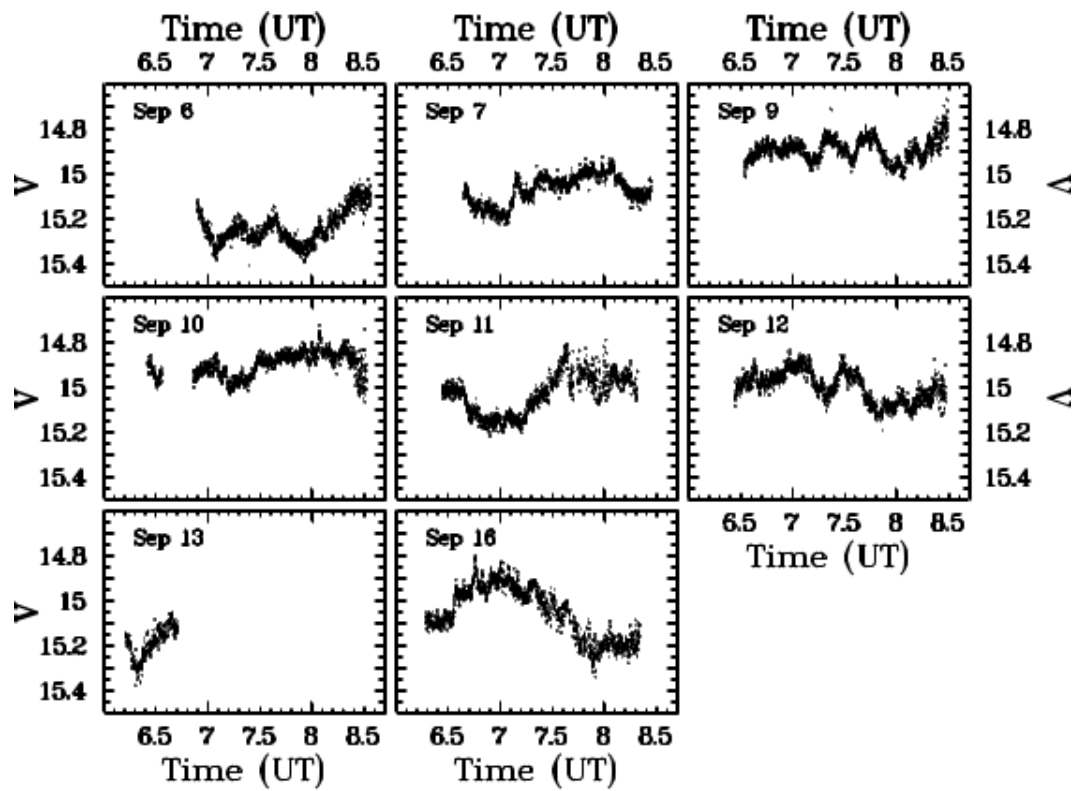


Figure 10: Light curves of AQ Men observed in 8 nights in 2018, September, all drawn on the same time and magnitude scale.



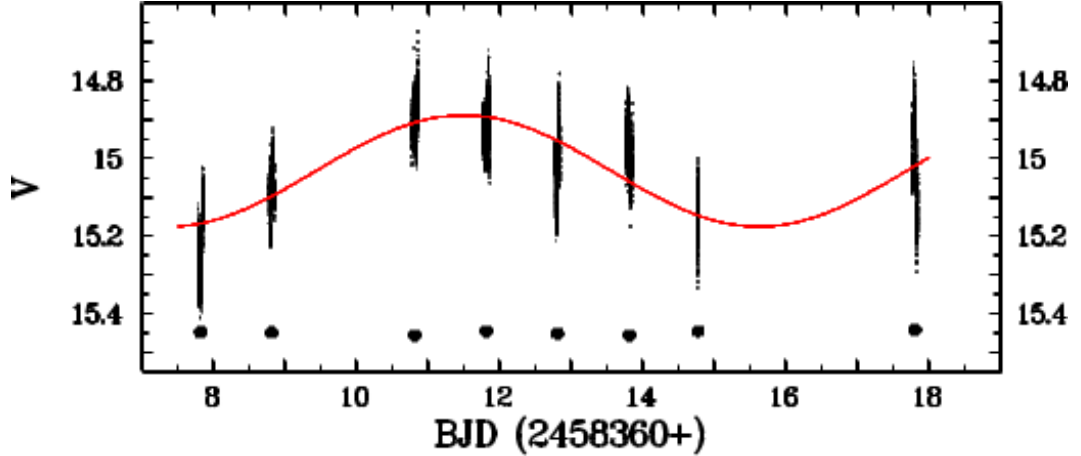


Figure 11: Combined light curves of AQ Men of 2018, September. The red curve is a least squares sine fit to the data. The filled circles represent the nightly averages of the magnitude difference between the comparison star to AQ Men and a check star (offset in magnitude by an arbitrary constant).

of 0.28 mag and a period of 8.25 d. However, the data covering a time interval only slightly longer than this period, it is impossible to say whether this modulation is really periodic or not. It occurs, in any case, on a time-scale significantly longer than the 3.78 d variation seen by Armstrong et al. (2013) which therefore cannot be a stable period of AQ Men. However, a visual inspection of the upper frame of fig. 1 of Armstrong et al. (2013) suggests, at least in the time interval BJD 2452000 – 40 a modulation on a similar time-scale as seen in the present data.

## 5.2 Variations on hourly time-scales

In order to verify if any of the spectroscopic or photometric periods seen by Chen et al. (2001) and Armstrong et al. (2013) can be detected in the present data, the night-to-night variations were first removed from the combined data set by subtracting the nightly average magnitudes. A power spectrum was then calculated. It is shown in Fig. 12 (black graph) and is dominated by the  $1 \text{ d}^{-1}$  alias patterns of several frequencies. In order to disentangle the effects of the window spectrum, the data were also submitted to the CLEAN algorithm (Roberts et al., 1987). The resulting spectrum is shown in red in the figure. The highest peak in both, the Lomb-Scargle periodogram and the CLEAN spectrum occurs at a frequency of  $f_0 = 12.276 \pm 0.031 \text{ d}^{-1}$ , where the error (here and in similar cases in Sections 6.1 and 8.1) is conservatively defined as the standard deviation of a Gaussian fit to the respective power spectrum peak in the Lomb-Scargle periodogram. There are several smaller peaks in the CLEAN spectrum. However, only the strongest survives if the CLEAN algorithm is run with different parameters (gain, number of iterations). Therefore, I do not consider them to be significant. But note that it is by no means guaranteed that the CLEAN algorithm chooses the correct period among the aliases (VanderPlas 2018). Thus, the power spectrum suggests that the light curve of AQ Men is modulated with a period of  $P = 1/(f_0 + n)$  where  $n$  is an integer. Choosing  $n = 0$  yields  $P_0 = 0.0814 \pm 0.0002 \text{ d}$  or  $1.954 \pm 0.005 \text{ h}$ . The light curve, folded on this period, is shown in Fig. 13, where the white ribbon represent the same data, binned in phase intervals of width 0.01. A formal sine-fit yields a full amplitude of

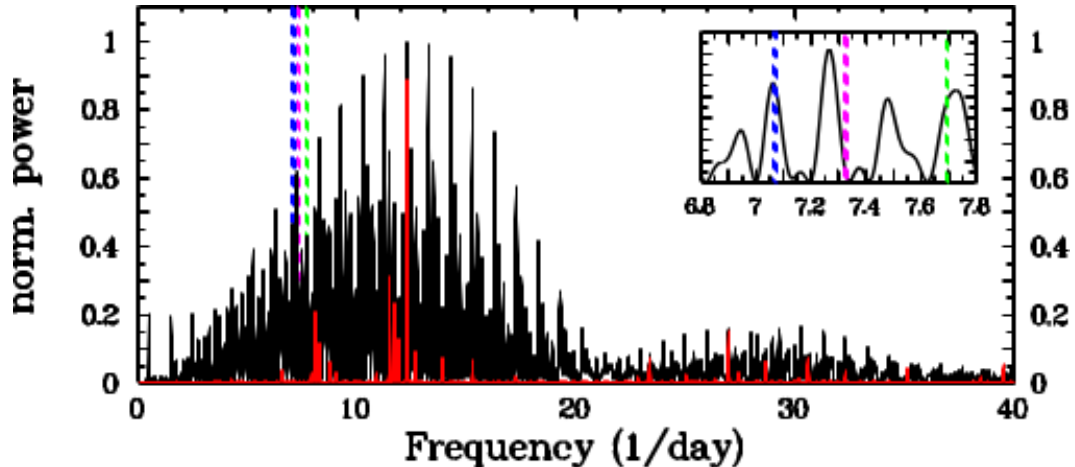


Figure 12: Normalized Lomb-Scargle periodogram (black) and CLEAN power spectrum (red) of the combined light curve of AQ Men of 2018, September, after subtracting the nightly average. The colour vertical lines indicate the frequency corresponding to the spectroscopic (green), eclipse (blue) and superhump (purple) periods, as quoted in the literature. The insert show a detail of the Lomb-Scargle periodogram around these frequencies.

0.13 mag for the variations.

How does the period found here relate to the other periods reported to be present in AQ Men? Not at all! The frequency corresponding to  $P_{\text{sp}}$ ,  $P_{\text{ecl}}$  and  $P_{\text{nSH}}$  are indicated in Fig. 12 by green, blue and purple, respectively, broken vertical lines. As can better be seen in the inset, which contains a blown up version of the power spectrum in a small range around these frequencies, there is a satisfactory coincidence of  $1/P_{\text{ecl}}$  with a minor power spectrum peak, a marginal coincidence of  $1/P_{\text{sp}}$  and no coincidence of  $1/P_{\text{nSH}}$ . Folding the light curves on any of these periods does not lead to convincing results. I could also not identify any simple arithmetic relationship between any of these frequencies and  $f_0$  or its aliases.

### 5.3 Discussion of the findings on AQ Men

The distance to AQ Men derived from the GAIA parallax is  $552 \pm 8$  pc (Bailer-Jones et al., 2018). The interstellar extinction is unknown. It should be between 0 and the total galactic extinction in the direction of the star. The reddening maps of Schlafly & Finkbeiner (2011) yield a total colour excess in the area around AQ Men of  $E_{B-V} = 0.148$ . Using the standard relation of  $A_V/E_{B-V} = 3.1$  this corresponds to a visual extinction of  $A_V = 0.46$ . The average magnitude of AQ Men during the present observations was  $V = 15.0$  (noting that this is only approximate because the observations were not calibrated). Thus, the absolute visual magnitude of AQ Men lies between 5.8 mag (if it suffers the full galactic extinction) and 6.3 mag (in the absence of any extinction). This is much brighter than the absolute magnitude of dwarf novae below the 2–3 h gap in the distribution of orbital periods of CVs (Warner, 1995), meaning that  $P_0$  is unlikely to be the revolution period of AQ Men. However it is compatible with the faint end of the absolute magnitude distribution of novalike variables. But then, the bulk of periods of these stars lies above the period gap. Could it be that the orbital light curve of AQ Men is double humped and the true period is  $2 \times P_0$ , raising it to about 4 h (considering possible alias values) and thus comfortably

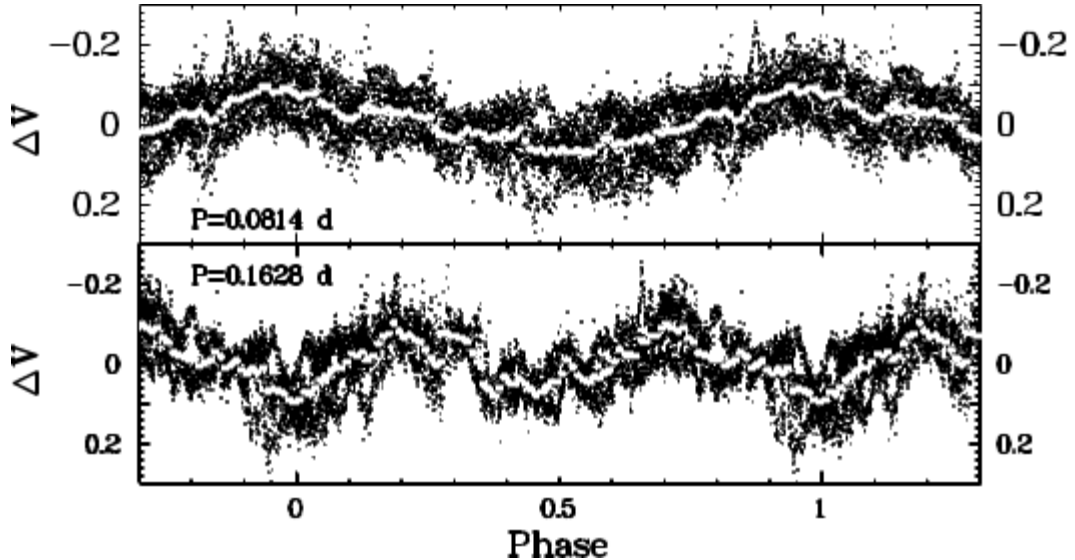


Figure 13: *Top*: Combined light curves of AQ Men of 2018, September, after subtracting the nightly average, folded on the period  $P_o = 0.0814$  d. The white ribbon represent the same data, binned in phase intervals of width 0.01. *Bottom*: The same, folded on  $2 \times P_o$ .

into the range populated by many novalike variables? The lower frame of Fig. 13, showing the lightcurve folded on  $2P_o$ , lends some credibility to this idea because the minima appear to have different depth. Such double-humped light curves are not unprecedented. They do not only occur in short period CVs as mentioned in Sect. 4.1 but also in systems with similar periods such as, for instance BD Pav (Barwig & Schoembs, 1983) ( $P_{\text{orb}} = 4.30$  h) and V367 Peg (Woudt et al., 2005) ( $P_{\text{orb}} = 3.88$  h). The difference between  $2P_o$  and  $P_{\text{sp}}$  is 2.3 times the error of the latter which, as mentioned earlier, may have been underestimated. Both periods may thus be considered compatible. However,  $2P_o$  is incompatible with  $P_{\text{ecl}}$ . Folding the present data on  $P_{\text{ecl}}$  in fact reveals a minimum which looks like an eclipse. But the evidence is insufficient because only one light curve covers the respective phase.

Thus, the present results cannot clarify the nature of the various photometric periods observed in AQ Men but rather complicate the picture.

## 6 LQ Pegasi

LQ Peg (= PG 2133+115) was discovered in the Palomar-Green survey (Green et al., 1986) and classified as a novalike variable by Ferguson et al. (1984). Most of the time it hovers at a magnitude of about 14.8 mag, but occasionally low states occur, as first seen by Sokolov et al. (1996) and then by Watanabe (1999), Kato & Uemura (1999), Schmidtke et al. (2002), and Kafka & Honeycutt (2005), testifying to a VY Scl nature of LQ Peg.

Not many details about the structure of the system are known. In particular, no time resolved spectroscopy has been performed. Based on regular brightness variations Papadaki et al. (2006) derived an orbital period of 0.124747 (6). However, even this is contested by Rude & Ringwald (2012) who argue that this period is rather due to a negative superhump. They consider the orbital period to be 0.1342 d. However, it was not observed directly in their photometry but inferred by two other periods of 0.1425 d (interpreted as a positive

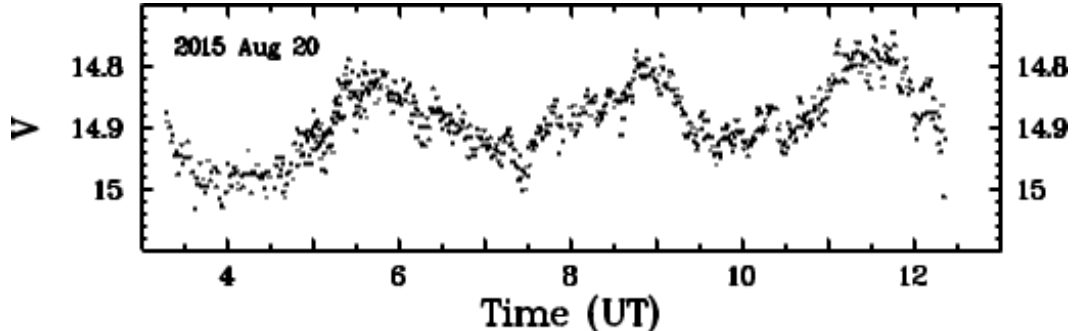


Figure 14: Light curve of LQ Peg of 2015 August 20, as an example of periodic light modulations in the system.

Table 2: Periods measured in the light curves of LQ Peg.

Dates	$N_{LC}^*$	$\Delta T^{**}$ (h)	Period
2004, Jun 1 ... Aug 30	10	44.9	$0.12474 \pm 0.00004$
2015, Aug 15 ... Sep 14	20	143.5	$0.12474 \pm 0.00021$
2016, Aug 16 ... Oct 16	17	103.2	$0.12491 \pm 0.00008$

\* Number of light curves

\*\* Total time base of light curves

superhump) and 2.37 d (thought to be the precession period of the accretion disk).

In an attempt to shed light upon the question of the orbital period, I re-analyse here the data of Papadaki et al. (2006), downloaded from the Centre de Donnée Astronomique de Strassbourg (CDS), consisting of 10  $R$  band and unfiltered light curves observed in 2004, June and August. These are complemented by 20 light curves obtained in 2015 August and September, and 17 light curves observed in 2016, August - October, retrieved from the AAVSO International Database. The latter refer to the  $V$  band. The median time resolution of all light curves is 60 s (range: 44 s – 125 s).

## 6.1 The period: Orbital or superhump?

All light curves of sufficient length clearly exhibit apparently periodic modulations. Fig. 14 shows an example. In order to investigate their stability and their nature as orbital or superhump variations the available data sets were divided into three groups according to the observing seasons mentioned earlier. Since part of the Papadaki et al. (2006) light curves were observed in  $R$  and others in white light, the average nightly magnitude was subtracted from the data just as has been done for the AAVSO data. The combined light curves of the three observing seasons were subjected to a periodogram analysis. The periods corresponding to the dominant peaks are summarized in Table 2. The periodogram of the 2004 data set contains two closely spaced alias peaks of very similar height caused by the window function. The choice between them is possible because the periodograms of the June and August subsets are free from this complication and – although of lower resolution – exclude within their formal errors one of the alias frequencies.

Graphs of the periodograms of the three data groups are shown in Fig. 15. In all cases they are dominated by a  $1 \text{ d}^{-1}$  alias pattern around a frequency close to the frequency corresponding to the period  $P_{\text{Pap}}$  measured by Papadaki et al. (2006) which is marked by

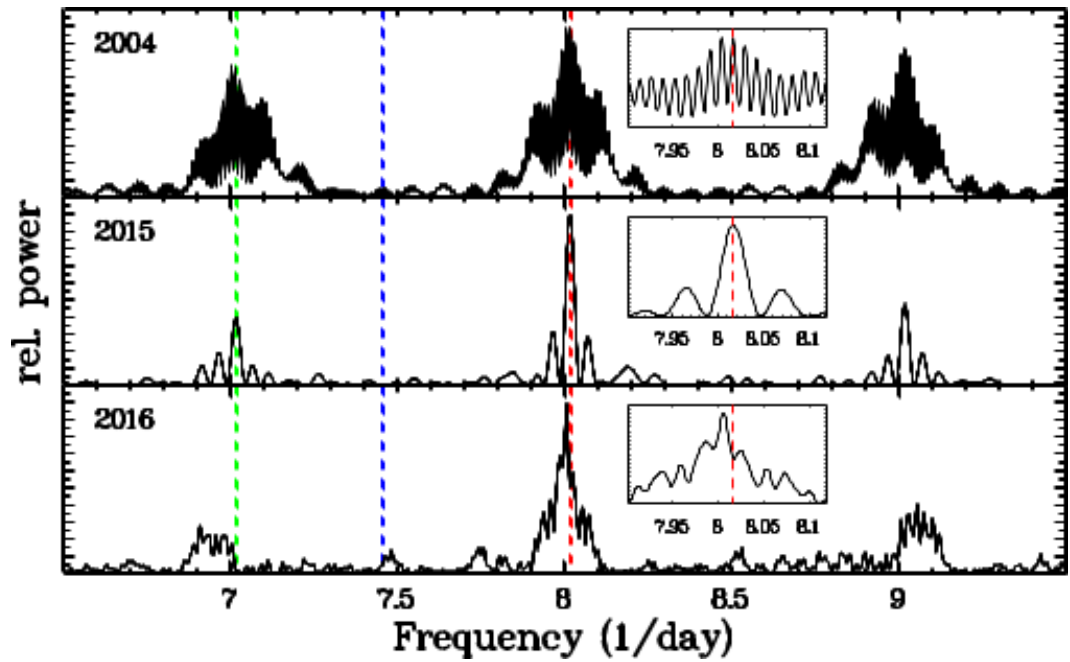


Figure 15: Periodograms of the combined light curves of LQ Peg obtained in three observing seasons. The inserts contain a blow-up of a small frequency range around dominant peak. The broken vertical lines indicate the frequencies of the period measured by Papadaki et al. (2006) (red, right), and the superhump (green, left) and orbital (blue, middle) periods suggested by Rude & Ringwald (2012).

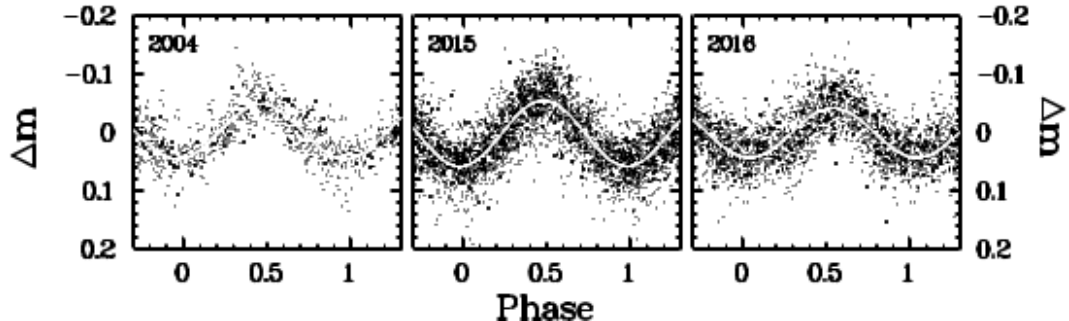


Figure 16: Seasonal light curves of LQ Peg folded on the dominant period. The white curves are least squares sine fits to the data.

the broken red (right) vertical line. The other lines indicate the frequencies of the superhump  $P_{\text{SH}}$  (green, left) and orbital period  $P_{\text{orb,RR}}$  (blue, middle) proposed by Rude & Ringwald (2012). The 2004 data are concentrated in two subgroups separated by more than two months, while those of the other years are more evenly distributed across the respective time base. Thus, the alias pattern in the 2004 periodogram contains more fine structure. This is particularly well visible in the inserts in Fig. 15 which contain a blow-up of a small frequency range around the Papadaki et al. (2006) period. Since the 2004 data are the same as investigated by Papadaki et al. (2006), it is not surprising that the frequency  $1/P_{\text{Pap}}$  is recovered as the highest peak in the periodogram. In 2015, the same frequency is dominating the periodogram. However, the dominant peak in 2016 is slightly offset from  $1/P_{\text{Pap}}$ . While it is still compatible with  $1/P_{\text{Pap}}$  on the  $2\sigma$  level (see Table 2), tests calculations using different subensembles of the 2016 data always yielded a peak frequency slightly smaller than  $1/P_{\text{Pap}}$ , making it unlikely that the difference is just due to statistical fluctuations. Moreover, folding the combined data on  $P_{\text{Pap}}$  reveals clear deviations from a smooth light curve. This lends some credibility to the notion that the dominant variations in the light curve of LQ Pap is indeed due to a superhump and not to the orbital motion. The superhump period suggested by Rude & Ringwald (2012) [the green (left) line in Fig. 15] is then a  $1 \text{ d}^{-1}$  alias of the true value. Considering the 2.37 precession period, the revised orbital period would then be 0.1185. However, I do not yet consider this small piece of evidence conclusive. Moreover, no signal is seen in the periodograms at the orbital frequency inferred by Rude & Ringwald (2012) or its revised value.

Thus the question whether the strong modulation seen in the light curves of LQ Peg is orbital in nature or is a superhump can, unfortunately, not be settled unequivocally by the present study. The seasonal data, folded on the period corresponding to the dominant periodogram peak, are shown in Fig. 16. The full amplitude of a sine fit to the data (white curves) is 0.09 mag in 2004 and 2016 and at 0.11 mag slightly higher in 2015.

## 6.2 The high frequency realm

Papadaki et al. (2006) suspect a hump to be present in their power spectrum of LQ Peg in the frequency range between  $26\text{--}45 \text{ d}^{-1}$ , suggesting the presence of QPOs. They recognize, however, that the signal is too weak to be certain. The larger number of light curves available here permits to address this question. The average of all power spectra of LQ Peg is shown (along with that of SS Cyg; see Sect. 4.2) on a log-log scale in Fig. 9. The broad hump at low frequencies is caused by the orbital (or superhump) variations. The frequency range of

the suspected QPOs extends between  $\log(f) = 1.41$  and  $1.65$ . The centre of this range is marked by an open red circle. There is no distinct feature in this range. Thus, the existence of the QPOs is not confirmed.

Instead, the red noise realm, caused by flickering, is well expressed and extends between  $1.15 < \log f < 2.4$  (red vertical bars in the figure). A linear least squares fit (red graph) yields a spectral index of  $1.24 \pm 0.04$  where the error is the standard deviation of  $\gamma$  derived from the three observing seasons. There is thus no significant change of  $\gamma$  over time. In contrast, Papadaki et al. (2006) quote very different nominal values. The difference, however, may not be significant because Papadaki et al. (2006) recognize that their  $\gamma$  depends on the exact definition of the fitting interval, leading to a wide uncertainty interval.

It should be noted that  $\gamma$  is significantly larger in SS Cyg compared to LQ Peg. This indicates a difference in the distribution of flickering power in the two systems: While in both of them the absolute value of the power grows at longer time-scales, the relative power of long lasting flares dominates more strongly over the power on short time-scales in SS Cyg compared to LQ Peg.

## 7 RW Trianguli

RW Tri is a deeply eclipsing novalike variable. The orbital period was determined by Robinson et al. (1991) to be  $0.231883297$  d. The inclusion of this system in the present study is motivated by the recent detection by Smak (2019) of a negative superhump present in light curves of RW Tri observed in 1957 and 1994. Moreover, albeit as a novalike variable RW Tri is not expected to undergo large magnitude variations (noting that low states such as those occurring in VY Scl stars have not been observed in this system), low amplitude ( $\approx 0.5$  mag) oscillations on the time-scale of some tens of days have been reported by Honeycutt et al. (1994) and Honeycutt (2001). The present data permit also to further explore this aspect.

A dense series of observations have been obtained by AAVSO observers during 2015-2016. It consists of 62 light curves observed between 2015, October 18 and 2016, February 9. They refer all to the  $V$  band. The total observing time amounts to 379 h, while the average length of individual light curves is 4.3 h (range: 1.8 h – 12.9 h). Their average time resolution is 61 s (range: 39 s – 86 s). Since I am interested here in variations other than eclipses, these have been removed from all data before further processing.

### 7.1 Long term variability

During a  $\approx 250$  d interval (out of a total of  $\approx 1000$  d of observations) during the 1992-1993 observing season Honeycutt et al. (1994) observed cyclic variations with a total amplitude of 0.45 mag and a period of 25.1 d (Honeycutt, 2001) in RW Tri. This is much more than eventual magnitude zero point problems in data taken with different instruments (see Sect. 2) can conceal. Therefore it is worthwhile to investigate the original AAVSO light curves (i.e., before subtracting the nightly average magnitude) for similar variations.

The larger density of the present data as compared to those of Honeycutt et al. (1994) permits a more rigorous characterization of the long term variations. The black dots in Fig. 17 represent average magnitudes of the nightly light curve. In particular during the first part of the observing season a very clear cyclic variability of the average magnitude is obvious which is lost when the season draws to an end. The red curve is a least squares sine fit to the average magnitudes before BJD 2457395. Its total amplitude of 0.47 mag is very similar to that seen by Honeycutt (2001), but at  $19.10 \pm 0.01$  d the period is somewhat

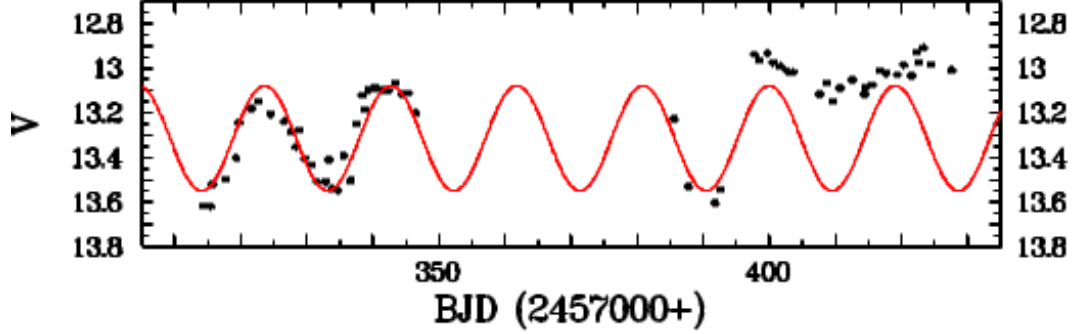


Figure 17: Long term light curve of RW Tri during the 2015-2016 observing season. The black dots represent the average magnitudes of the nightly light curves. The red curve is a least squared sine fit to the data before BJD 2457395.

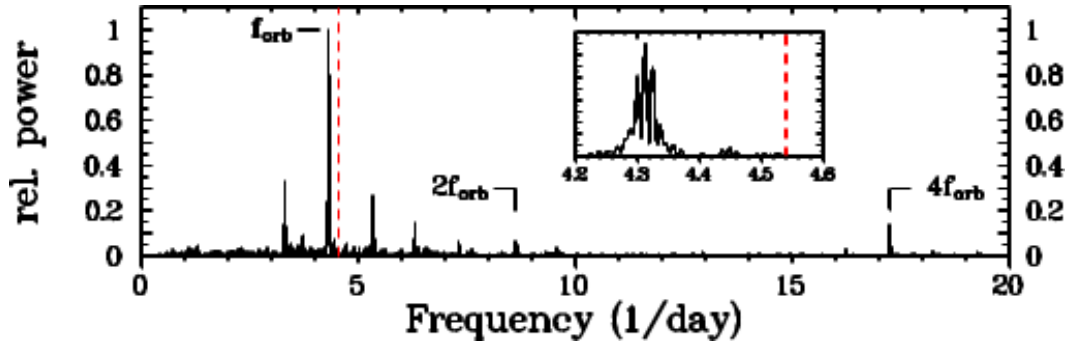


Figure 18: Lomb-Scargle periodogram of the combined light curves of RW Tri. The broken vertical line indicates the frequency of the negative superhump reported by Smak (2019). The insert shows the region around the superhump and orbital frequencies on an amplified scale.

shorter. After BJD 2458395 the system brightens slightly and the amplitude of the variations decreases significantly. However, at least for another 19 d cycle their phase is maintained.

## 7.2 Superhumps in RW Tri?

Recently, Smak (2019) reported the detection of a negative superhump at a period of 0.2203 d (i.e., 5% shorter than the orbital period) in light curves of RW Tri observed in 12 nights in September 1994. Some indications for the superhump were also found in 4 light curves taken in November-December 1957. If this feature is real and persistent, as it is for instance in TT Ari (Bruch 2019), it should easily be revealed in the present data. However, it is not.

To study this issue, I now employ the RW Tri light curves after subtraction of the nightly average magnitude. A Lomb-Scargle periodogram of the combined data was calculated. Since there is a gap of 40 d in the long term light curve (see Fig. 17) I also investigated the data before and after the gap separately. The results were almost identical.

The power spectrum is displayed in Fig. 18. Significant peaks appear at the orbital frequency  $f_{\text{orb}}$ , twice this value and, somewhat surprisingly and with considerable strength,  $4f_{\text{orb}}$ . Several  $1 \text{ d}^{-1}$  aliases of these features are also obvious. All other structures which may be considered at the brink of significance, can be traced to only one of the two parts of the



total data set and therefore do not reflect persistent variations in RW Tri. Indeed, subtracting the average waveform from the combined data, the power spectrum of the resulting light curve does not contain convincing evidence for a residual periodic signal.

In particular, no trace of a superhump is present. Its frequency, as measured by Smak (2019) is marked by a broken vertical line in Fig. 18. The absence of the superhump signal is even more evident in the insert which shows the corresponding spectral region, also including the orbital frequency, on an amplified scale. The satellite peaks of the orbital maximum can be explained as beat frequencies with the total observing window.

Thus, it must be concluded that at least during the 2015-2016 observing season no evidence of a negative superhump in RW Tri exists.

## 8 UX Ursae Majoris

UX UMa is another well known deeply eclipsing novalike variable. At 0.196671278 d (Baptista et al., 1995) it has an orbital period only slightly smaller than RW Tri. I include UX UMa in this study because based on an extensive observing campaign in 2015 de Miguel et al. (2016) recently found a modulation with a period of 3.680 d in its light curve which they interpret as being due to a retrograde precession of the accretion disk. An associated negative superhump at the beat period of the precession and the orbit is also seen at 0.186700 d. At the end of the discussion of their observations de Miguel et al. (2016) remark (citing): *So it's a decent bet, though by no means sure, that these superhump effects have been lurking, unsuspected, in many previous observations of UX UMa.* As I will show below, they loose their bet. At least, the presence of superhumps is not a common phenomenon in UX UMa, but rather an exception.

I use a total of 198 light curves covering a total time base of 1133 h, observed during several observing seasons. They were all retrieved from the AAVSO International Database and refer to the  $V$  band. The eclipses were removed. A summary of these observations is given in Table 3, where the number of light curves and the total time base is listed as a function of observing season. The majority of the observations is concurrent with those analysed by de Miguel et al. (2016) and – although they did not provide a detailed list of their observations, so that a direct comparison is not possible – I suspect that at least some (or even most) of the data studied here are the same as those used by them. Since these light curves cannot provide much information beyond the more detailed investigation of de Miguel et al. (2016), the 2015 data are only briefly treated in Sect. 8.1 in order to verify the previous results, before the data of other observing seasons are regarded in Sect. 8.2 in the quest for the presence of superhumps at other epochs.

### 8.1 2015

The analysis of the 2015 data fully confirms the results of de Miguel et al. (2016). The are summarized in Fig. 19 and Table 4. The figure (main frame) shows the intermediate frequency range of the power spectrum of the combined light curves of UX UMa after subtraction of the nightly average magnitude, while the insert is a blow-up of the low frequency part, using the data before subtracting the average. The table lists the frequencies (and periods) of the main power spectra peaks (in the order of their relative strength).

At low frequencies, two independent signals are seen.  $f_{11}$  is the prominent variation interpreted by de Miguel et al. (2016) as due to disk precession. The second signal at  $f_{12}$  (corresponding to a period of 18.8 d) appears to be somewhat clearer in the present data than, e.g., in fig. 2 of de Miguel et al. (2016) who suspected it to be spurious. I am more

Table 3: Summary of UX UMa light curves per observing season

Year	$N_{LC}^*$	$\Delta T^{**}$ (h)
2005	7	26.8
2012	5	31.9
2013	17	96.3
2014	23	193.7
2015	112	649.5
2016	10	38.2
2017	13	40.8
2018	11	52.3

\* Number of light curves

\*\* Total time base of light curves

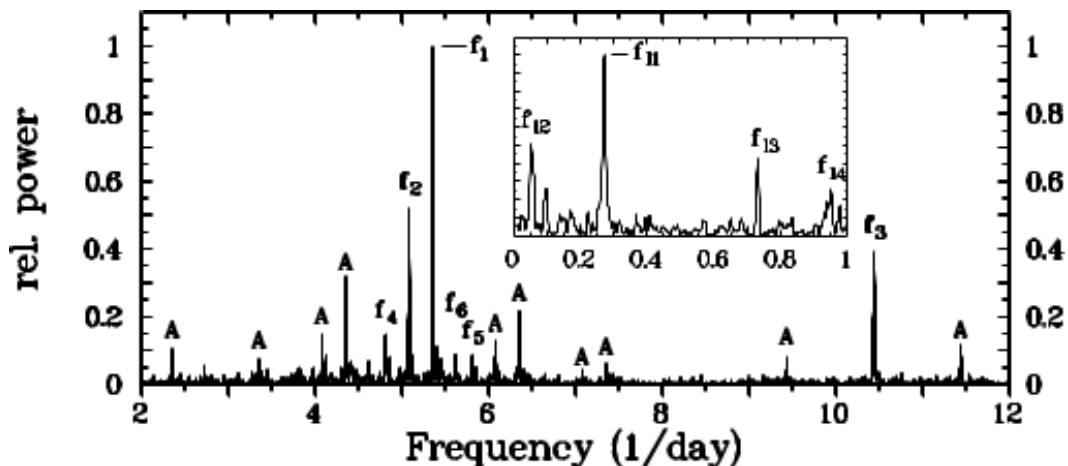


Figure 19: Lomb-Scargle periodogram of the combined light curves of UX UMa. The main significant peaks are identified and discussed in the text. Obvious  $1 \text{ d}^{-1}$  aliases are labelled as “A”. The insert contains the low frequency part of the periodogram of the combined data before subtracting the nightly average magnitude.

inclined to consider the reality of a period or quasi-period close to 19 d an open issue.  $f_{13}$  and  $f_{14}$  are obviously caused by a beat of  $f_{11}$  and  $f_{12}$  with the window spectrum which has a strong maximum at  $1 \text{ d}^{-1}$ .

At first glance, the power spectrum at intermediate frequencies (main frame of Fig 19) appears confusing. However, it is really quite simple. Apparently significant signals are labelled  $f_1 - f_6$ , while obvious  $1 \text{ d}^{-1}$  aliases are identified by an “A”. The main peak at  $f_1$  is the beat between the precession frequency and the orbital frequency  $f_2$ , i.e., the negative superhump frequency. All other signals can be interpreted as sums or differences between the orbital and the precession frequency, as detailed in Table 4. Thus, disregarding  $f_{12}$ , the light curve of UX UMa contains only two independent frequencies: the orbital and the precession (or, alternatively, the superhump) frequency.

Table 4: Frequencies (in  $\text{d}^{-1}$ ) and periods (in d) in the 2015 power spectrum of UX UMa

Low ( $< 1\text{d}^{-1}$ ) frequency range:		
$f_{l1} = 0.2719 \pm 0.0039$	$P_{l1} = 3.676 \pm 0.053$	
$f_{l2} = 0.0531 \pm 0.0035$	$P_{l2} = 18.82 \pm 1.2$	
$f_{l3} = 0.7399 \pm 0.0036 \equiv 1 - f_{l1}$		
$f_{l4} = 0.9491 \pm 0.0038 \equiv 1 - f_{l2}$		
Intermediate ( $2\text{--}12\text{d}^{-1}$ ) frequency range:		
$f_1 = 5.3573 \pm 0.0046 \equiv f_2 - f_{l1}$		
$f_2 = 5.0835 \pm 0.0036$	$P_2 = 0.196715 \pm 0.00014$	
$f_3 = 10.4059 \pm 0.0052 \equiv 2f_1 - f_{l1}$		
$f_4 = 4.8123 \pm 0.0059 \equiv f_2 - f_{l1}$		
$f_5 = 5.8146 \pm 0.0053 \equiv f_2 + f_{l1}$		
$f_6 = 5.6179 \pm 0.0030 \equiv f_1 + f_{l1}$		

## 8.2 Other observing seasons

To which degree the behaviour of UX UMa observed in 2015 repeats itself at other epochs? In order to answer this question, Fig. 20 (left column) contains the power spectra of the combined light curves observed in 8 different seasons [including the 2015 season (in blue) to facilitate the comparison]. The orbital frequency and its first overtone is indicated by the red broken vertical lines. It must be taken into account that the number of light curves in all other years is considerably smaller than in 2015. Thus, non-periodic variations together with the random distribution of data within the observing season, cause a multitude of structures in the power spectrum and any real periodic signal will be less outstanding. Significant peaks (together with their  $1 \text{ d}^{-1}$  aliases) are always (except in 2015) seen at the first harmonic of the orbital frequency  $f_2$  and in general, but often at a reduced strength, at  $f_2$  itself. In no year other than 2015 any indication of the negative superhump at  $f_1$  is seen. In 2016, a peak close to  $f_3$  appears. However, the absence of any convincing signal at  $f_1$  – so much stronger than  $f_3$  in 2015 – and the presence of many other peaks of similar strength makes it doubtful that it really reflects the presence of a superhump.

The right column of Fig. 20 contains the seasonal light curves folded on the orbital period, binned in phase intervals of width 0.01. The average orbital waveform consists of a more or less well defined hump encompassing roughly the first 2 thirds of the orbit, followed by a stronger hump, canonically considered as the manifestation of the hot spot in high inclination CVs. Only in 2015 the waveform is drastically different (see also fig. 3 of de Miguel et al., 2016).

Thus, both, the power spectra and the average orbital waveform, clearly indicate that the photometric behaviour of UX UMa observed in 2015 is not seen during any other observing season investigated here. It must therefore be regarded as exceptional. This evidently leads to the question of the reason for the emergence of the unusual light curve in 2015 and, assuming that its interpretation by de Miguel et al. (2016) is correct, the change of structure of the accretion disk. This question, however, will not be answered here.

## 9 Conclusions

The purpose of this paper is to verify and expand on previous published details of miscellaneous variations observed in some cataclysmic variables. It also shows the value of archival

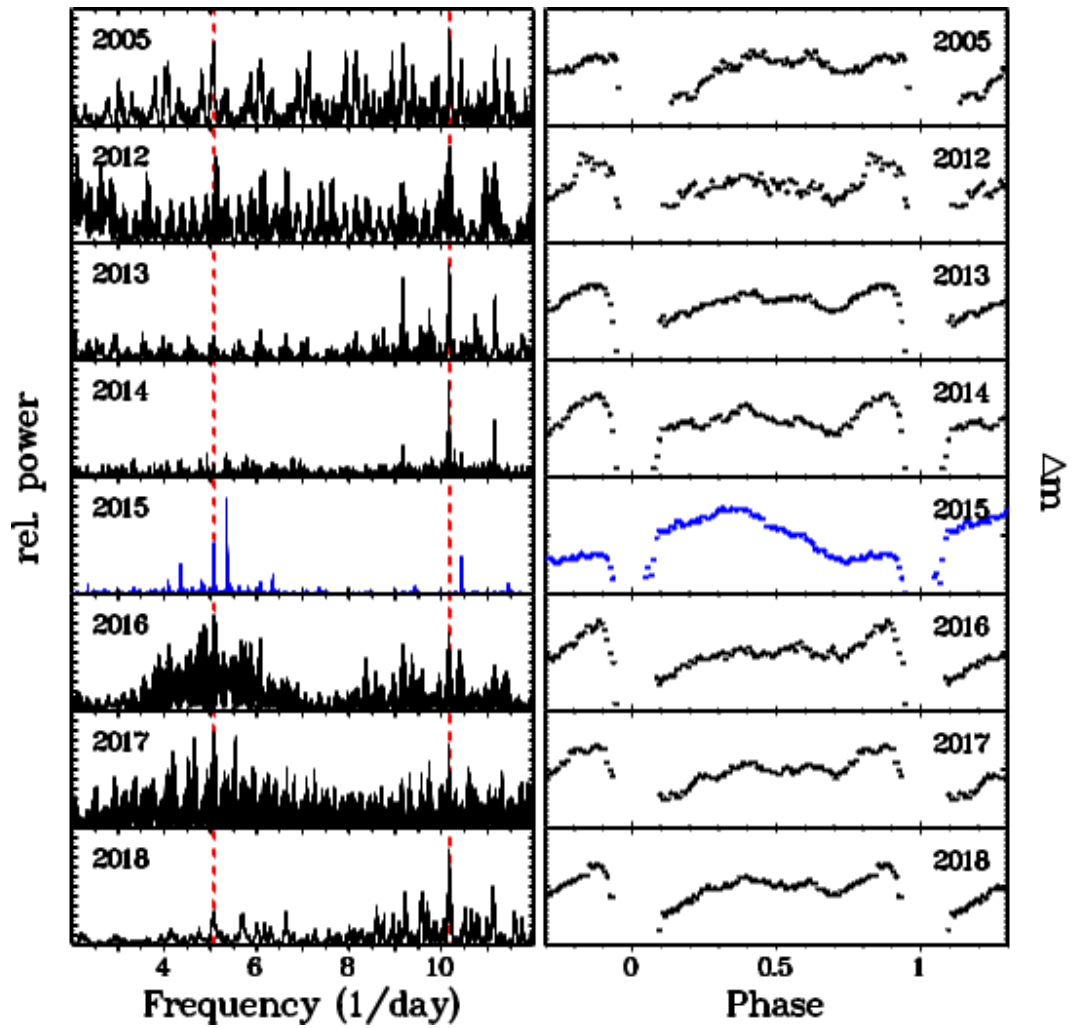


Figure 20: *Left:* Lomb-Scargle periodograms of the combined light curves of UX UMa in different years. The broken vertical lines indicate the orbital frequency and its first overtone. *Right:* The combined seasonal light curves folded on the orbital period, binned in intervals of with 0.01 in phase.

data, which are readily available but have not yet been exploited adequately. The main findings can be summarized as follows:

*V455 And:* Improved orbital ephemerides are presented. Claims of a positive superhump during quiescence cannot be substantiated since the corresponding variations can be explained as a aliasing effect with orbital variations. On the other hand, the continuous presence of negative superhumps is confirmed. The variations of the frequencies of non-radial pulsations of the white dwarf over the years suggest that in 2008 the star was still too hot after the 2007 outburst to exhibit pulsations and that it has reached its equilibrium temperature by 2012. Pulsations are not stable but can rapidly appear and disappear or change their frequencies.

*SS Cyg:* The waveform of the double humped orbital variations changed from year to year in the sense that the fainter hump occurring during the first half of the orbit may all but vanish or may almost reach the amplitude of the stronger second maximum. Previous claims for a dependence of the waveform on the phase within the outburst cycle of SS Cyg cannot be confirmed. The same is true for 12 min oscillations which have been claimed to be evidence for an intermediate polar nature of SS Cyg.

*AQ Men:* Variations of the system brightness with a period of  $\approx 8$  days (which, however, requires confirmation) are seen. A modulation of the light curve with a period of about 2 h (or twice this value) is also observed. Its nature is not clear. None of the brightness changes of AQ Men could be related to previously determined photometric or spectroscopic periods.

*LQ Peg:* Conflicting interpretations in the literature concerning cyclic modulations in this star as being orbital or superhump variations could not unambiguously be resolved. QPOs have been suspected previously to occur in LQ Peg. The present observations do not contain any indication for their presence.

*RW Tri:* A negative superhump claimed to have been observed in 1994 and possibly in 1957 is definitely not a permanent feature since no trace could be seen in extensive data obtained during 2015-16. On the other hand, the occasional occurrence of cyclic variations on the time-scale of  $\approx 20$  d is confirmed at a much higher confidence level than permitted by previous reports.

*UX UMa:* The unusual photometric behaviour of UX UMa, exhibiting a negative superhump and variations on the precession period of a warped accretion disk in 2015, is confirmed. But it is also shown that this behaviour is unusual and does not repeat in none of the seven other observing seasons for which data are available.

## Acknowledgements

This work is partly based on observations taken at the Observatório do Pico dos Dias operated by the Laboratório Nacional de Astrofísica, Brazil. It also depends to a great deal on archival data downloaded from the AAVSO International Database. I thank the numerous dedicated observers of the AAVSO for their contributions, together with the AAVSO staff for maintaining the database. Without their efforts this work would not have been possible. This research made also use of the VizieR catalogue access tool, CDS, France (DOI: 10.26093/cds/vizier).

## References

- Araujo-Betancor, S., Gänsicke, B.T., Hagen, H.-J., et al., 2005, *A&A*, 430, 629
- Armstrong, E., Patterson, J., Michelsen, E., et al., 2013, *MNRAS*, 435, 707

Bailer-Jones, C. A. L., Rybizki, J., Fouesneau, M., Mantelet, G., Andrae, R., 2018, *AJ*, 156, 58  
 Baptista, R., Horne, K., Hilditch, R.W., Mason, K.O., Drew J.E., 1995, *ApJ*, 448, 395  
 Bartolini, C., et al., 1985, *Mbga.conf*, 50,  
 Barwig H., Schoembs R., 1983, *A&A*, 124, 287  
 Bitner, M.A., Robinson, E.L., Behr, B.B., 2007, *ApJ*, 662, 564  
 Bloemen, S., Steeghs, D., De Smedt, K., et al., 2013, *MNRAS*, 429, 3433  
 Bruch, A., 1990, *AcA*, 40, 369  
 Bruch, A., 2014, *A&A*, 566, A101  
 Bruch, A., 2018, *NewA*, 58, 53  
 Bruch, A., 2019, *MNRAS*, 489, 2961  
 Chen, A., O'Donoghue, D., Stobie, R.S., Kilkenny, D., Warner, B., 2001, *MNRAS*, 325, 89  
 de Miguel, E., Patterson, J., Cejudo, D., et al., 2016, *MNRAS*, 457, 1447  
 Eastman, J., Siverd, R., Gaudi, B.S., 2010, *PASP*, 122, 935  
 Ferguson, D.H., Green, R.F., Liebert, J., 1984, *ApJ*, 287, 320  
 Gänsicke, B.T., 2007, *ASPC*, 597, *ASPC..372*  
 Giovannelli, F., Sabau-Graziati, L., 2012, *MmSAI*, 83, 698  
 Green, R.F., Schmidt, M., Liebert, J., 1986, *ApJS*, 61, 305  
 Hagen, H.-J., Groote, D., Engels, D., Reimers, D., 1995, *A&AS*, 111, 195  
 Hessman, F.V., Robinson, E.L., Nather, R.E., Zhang, E.-H., 1984, *ApJ*, 286, 747  
 Honeycutt, R.K., 2001, *PASP*, 113, 473  
 Honeycutt, R.K., Robertson, J.W., Turner, G.W., Vesper, D.N., 1994, *ASPC*, 277, 56  
 Kafka, S., Honeycutt, R.K., 2005, *IBVS*, 5597, 1  
 Kato, T., Imada, A., Uemura, M., et al., 2009, *PASJ*, 61, S395  
 Kato, T., Uemura, M., 1999, *IBVS*, 4786, 1  
 Kjurkchieva, D., Marchev, D., Drozd, M., 1998, *Ap&SS*, 262, 453  
 Kozhevnikov, V.P., 2015, *NewA*, 41, 59  
 Lomb, N.R., 1976, *Ap&SS*, 39, 447  
 Maehara, H., Imada, A., Kubota, K., et al., 2009, *ASPC*, 57, 404  
 Matsui, R., Uemura, M., Arai, A., et al., 2009, *PASJ*, 61, 1081  
 Mukadam, A.S., Pyzas, S., Townsley, D.M., et al., 2016, *ApJ*, 821, 14  
 Nogami, D., Hiroi, K., Suzuki, Y., et al., 2009, *ASPC*, 52, 404  
 Papadaki, C., Boffin, H.M.J, Sterken, C., et al., 2006, *A&A*, 456, 599  
 Patterson, J., Stone, G., Kemp, J., et al., 2018, *PASP*, 130, 064202  
 Roberts, D.H., Lehar, J., Dreher, J.W., 1987, *AJ*, 93, 968  
 Robinson, E.L., Shetrone, M.D., Africano, J.L., 1991, *AJ*, 102, 1176  
 Rude, G.D., Ringwald, F.A., 2012, *NewA*, 17, 453  
 Scargle, J.D., 1982, *ApJ*, 263, 835  
 Schlafly, E.F., Finkbeiner, D.P., 2011, *ApJ*, 737, 103  
 Schmidtke, P.C., Ciudin, G.A., Indlekofer, U.R., et al., 2002, *ASPC*, 539, 26  
 Silvestri, N.M., Szkody, P., Mukadam, A.S., et al., 2012, *AJ*, 144, 84  
 Smak, J., 2019, *AcA*, 69, 79  
 Sokolov, D.A., Shugarov, S.Y., Pavlenko, E.P., 1996, *ASSL*, 219, 208  
 Szkody, P., Mukadam, A.S., Gänsicke, B.T., et al., 2013, *ApJ*, 775, 66

VanderPlas, J.T., 2018, ApJS, 236, 16  
 Voloshina, I.B., 1986, PAZh, 12, 219  
 Voloshina, I.B., Khruzina, T.S., 2000, ARep, 44, 89  
 Voloshina, I.B., Lyutyi, V.M., 1983, PAZh, 9, 612  
 Voloshina, I.B., Lyutyi, V.M., 1993, ARep, 37, 34  
 Warner, B., 1995, *Cataclysmic Variables Stars*, Cambridge University Press  
 Watanabe, T., 1999, SVOLJ Var. Star Bull., 34, 3  
 Woudt, P.A., Warner, B., Spark, M., 2005, MNRAS, 364, 107  
 Zacharias, N., Finch, C.T., Girard, T.M., et al., 2013, AJ, 145, 44  
 Allen, C.W. 1973, *Astrophysical Quantities*, third edition (Athlone Press: London)  
 Baptista, R. 2012, Mem.S.A.It., 83, 530  
 Bateson, F.M. 1974, Publ. Var. Star Sect., RASNZ, 2, 1  
 Brown, A.G.A, Vellenari, A., Prusti, T., et al. 2016, A&A, 595, A2  
 Bruch, A. 1993, MIRA: A Reference Guide (Astron. Inst. Univ. Münster)  
 Bruch, A. 2016, New Astr., 46, 90  
 Bruch, A. 2017a, New Astr., 52, 112  
 Bruch, A. 2017b, New Astr., in press  
 Bruch, A., & Diaz, M.P. 2017, New Astr., 50, 109  
 Caceci, M.S., & Cacheris, W.P. 1994, Byte, May 1984, 340  
 Catalán, S., Isern, J., García-Berro, E., & Ribas, I. 2008, MNRAS 387, 1693  
 Claret, A., & Bloemen, S. 2011, A&A, 529, A75  
 Durašević, G., Latković, O., Vince, I., & Cséki, A. 2010, MNRAS, 409, 329  
 Durašević, G., Vince, I., Antokhin, I.I., et al. 2012, MNRAS, 420, 3081  
 Eastman, J., Siverd, R., & Gaudi, B.S. 2010, PASP, 122, 935  
 Eggleton, P.P. 1983, ApJ, 268, 368  
 Evans, P.A., Beardmore, A.P., Osborne, J.P., & Wynn, G.A. MNRAS, 399, 1167  
 FitzGerald, M.P. 1970, A&A, 4, 234  
 Garrido, H.E., Mennickent, R.E., Durašević, G., et al. 2013, MNRAS, 428, 1594  
 Gicger, A. 1987, Acta Astron., 37, 29  
 Goliašch, J., & Nelson, L. 2015, ApJ, 809, 80  
 Harmanec, P., & Scholz, G. 1993, A&A, 279, 131  
 Hoffman, D.J, Harrison, T.E., Coughlin, J.L., et al. 2008, AJ, 136, 1067  
 Høg, E., Fabricius, C., Makarov, V.V., et al. 2000, A&A, 355, L27  
 Houk, N. 1978, *Catalogue of two dimensional spectral types for the HD stars*, Vol. 2, University of Michigan  
 Jacoby, G.H., Hunter, D.A., & Christian, C.A. 1984, ApJ Suppl., 56, 257  
 Kalomeni, B., Nelson, L., Rappaport, S., et al. 2016, ApJ, 833, 83  
 Kazarovetz, E.V., Samus, N.N., Durlevich, O.V., Kireeva, N.N., & Pastukhova, E.N. 2008, IBVS 5863  
 Kilkeny, D., & Laing, J.D. 1990, SAAO Circ., 14, 11  
 Kordopatis, G., Gilmore, G., & Steinmetz, M. 2013, AJ, 146, 134  
 Lasota, J.-P. 2001, New Astron. Rev., 45, 449  
 Mennickent, R.E., & Djurašević, G. 2013, MNRAS, 432, 799

- Mennickent, R.E., Durašević, G., Kołaczkowski, Z., & Michalska, G., 2012, MNRAS, 421, 862
- Menzies, J.W., O'Donoghue, D., & Warner, B. 1986, ApSS, 122, 73
- Nauenberg, M. 1972, ApJ, 175, 417
- Osaki, Y. 1996, PASP, 108, 39
- Pezzuto, S., Bianchini, A., & Stagni, R. 1996, A&A, 312, 865
- Paczyński, B., & Schwarzenberg-Czerny, A. 1980, Asta Astron, 30, 127
- Pojmanski, G. 2002, Acta Astron, 52, 397
- Rafert, J.B., & Twigg, L.W. 1980, MNRAS, 193, 79
- Ritter, H. 2010, Mem. S.A.It., 81, 849
- Ritter, H., & Kolb, U. 2003, A&A, 404, 301
- Salaris, M., Serenelli, A., Weiss, A., & Miller Bertolami, M. 2009, ApJ, 692, 1013
- Shears, J., & Poyner, G. 2009, JBAA, 120, 169
- Smak, J. 1983, ApJ, 272, 234
- Szkody, P., & Mattei, J.A. 1984, PASP, 96, 988
- Walter, F., Bond, H.E., & Pasten, A. 2006, IAU Cir. 8663
- Warner, B. 1987, MNRAS, 227, 23
- Warner, B. 1995, Cataclysmic Variable Stars, Cambridge University Press, Cambridge
- Wilson, R.E. 1979, ApJ, 234, 1054
- Wilson, R.E., & Devinney, E.J. 1971, ApJ, 166, 605
- Zacharias, N., Finch, C.T., Girard, T.M., et al. 2013, AJ, 145, 44
- Zhao, J.K., Oswalt, T.D., Willson, L.A., Wang, Q., & Zhao, G. 2012, ApJ, 746, 144
- Zorotovic, M., Schreiber, M.R., & Gänsicke, B.T. 2011, A&A, 536, A42
- Zwitter, T., & Munari, U. 1995, A&AS, 114, 575
- Zwitter, T., & Munari, U. 1996, A&AS, 117, 449